Comprehensive Study on Congo Red Removal Using Natural Adsorbent: Characterization, Box-Behnken Design, Isotherm Modeling, and Cost Analysis

F. Benyahia,[a,c,*] A. Boudaoud,[b] M. Benalia,[c] M. Djedid,[c] and I. Nouacer[c]

[a]Department of Process Engineering, Laboratory of Process Engineering (LGP), Laboratory of Process Engineering, Materials and Environmental (LPEME), Faculty of Technology, Amar Telidji University of Laghouat, Laghouat, Algeria

[b]Department of The Common Trunk Sciences and Technology, Laboratory of Process Engineering, Materials and Environmental (LPEME), Faculty of Technology, Amar Telidji University of Laghouat, Laghouat, Algeria

[c]Department of Process Engineering, Laboratory of Process Engineering, Materials and Environmental (LPEME), Faculty of Technology, Amar Telidji University of Laghouat, Laghouat, Algeria

doi: https://doi.org/10.15255/CABEQ.2025.2475

Original scientific paper
Received: December 18, 2025
Accepted: May 4, 2026

In the present paper, the potential of a locally sourced plant-based adsorbent, *Ziziphus lotus* stone, for the removal of Congo Red (CR) dye from aqueous media was evaluated. The adsorbent was characterized using X-ray diffraction (XRD), Fourier-transform infrared spectroscopy (FTIR), scanning electron microscopy (SEM)/energy-dispersive X-ray spectroscopy (EDS), thermogravimetric analysis (TGA), differential scanning calorimetry (DSC), and Brunauer-Emmet-Teller (BET) surface area analysis. These combined characterization methods provided a comprehensive profile of the material, confirming the presence of active surface functional groups, a porous structure and high thermal stability. The BET surface area was estimated at 4.7758 $m^2\ g^{-1}$, with a pore size of 4.3578 nm. About 10 % enhancement in the adsorption efficiency of Congo Red dye was achieved using response surface methodology (RSM) based on the Box-Behnken Design (BBD), considering three key factors: adsorbent dose, pH, and initial CR dye concentration. As a result, the overall adsorption efficiency reached up to 95 %. The isotherm study, based on non-linear isotherm models, indicated that the adsorption data were best described by the Freundlich model, with maximum adsorption capacity Q_{max} of 11mg g^{-1}. Thermodynamic analysis revealed negative values of ΔG^0, ΔH^0 (–11.0959 kJ mol^{-1}), and ΔS^0 (–29.587 J K^{-1} mol^{-1}), indicating that the adsorption process was exothermic, spontaneous, and accompanied by decreased randomness at the solid-liquid interface. Furthermore, a techno-economic assessment of the based-plant adsorbent and the overall adsorption process was conducted. The estimated production cost of the *Ziziphus lotus* stone adsorbent was estimated at around 0.11304 USD/kg, while the overall adsorption cost was approximately 0.112 USD/m^3. These findings confirm the viability and high efficiency of *Ziziphus lotus* stone as a low-cost adsorbent for large-scale and low-cost environmental applications.

Keywords

agricultural waste, adsorption, Congo Red, BBD Design, process optimization, cost estimation

Introduction

The detrimental effects of pollution across multiple environmental compartments, including air, soil, and water, constitute a critical global challenge that threatens ecosystems, public health, and long-term sustainability. Rapid population growth, together with the accelerated industrial development, has intensified pollutant emissions and accelerated the depletion of natural resources[1,2]. Among the various forms of environmental pollution, wastewater contamination and declining water quality remain major concerns. Increasing water pollution has profound adverse effects on freshwater security, promotes the spread of waterborne diseases, and threatens the sustainability of ecological and economic systems[3,4]. In this context, the extensive use of syn-

*Corresponding author:
fa.benyahia@lagh-univ.dz; fatma.benyahia@lagh-univ.dz

thetic dyes and pigments across multiple industries, such as tannery, textiles, rubber, coatings, plastics, cosmetics, and pharmaceuticals[5], has become a significant environmental and human health issue. The discharge of untreated textile effluents into the environment creates severe risks to the ecosystems and human health[6,7], especially since about 30 % of dye production may be wasted during the manufacturing process[8]. The textile industry, one of the most water-intensive industrial sectors worldwide, relies heavily on processes such as dyeing and finishing[9], employing a wide variety of dyes, including reactive, acid, direct, disperse, vat, and azo dyes[9]. Among these, azo dyes represent the most widely used class of dyes, constituting nearly 50 % of annual global dye production and approximately two-thirds of all synthetic dyes[10]. In particular, azo dyes contain azo linkages (–N=N–) attached to aromatic rings and sulfonate groups ($–SO_3^-$). Under anaerobic conditions, these compounds can transform into even more hazardous byproducts, posing serious ecological and health risks[10].

Congo Red (CR) dye is an aromatic diazo dye with the chemical formula $C_{32}H_{22}N_6Na_2O_6S_2$ and a molecular mass of 696.68 g mol^{-1}, reflecting its complex framework. CR exhibits remarkable stability and resistance to biodegradation and photodegradation[10,11]. Consequently, CR is widely used in diverse industrial sectors, notably rubber, plastics, paper, and textiles, because of its intense scarlet color, high stability, and water solubility[5]. The discharge of textile wastewater containing high concentrations of CR significantly contributes to environmental pollution and poses serious health hazards. CR exhibits a complex molecular architecture characterized by acidic auxochromes, namely sulfonate groups ($–SO_3^-$) that impart a negative charge (anionic features), together with two azo chromophores (–N=N–) connected to two symmetric aromatic rings[12]. Under anaerobic conditions, including those present in the human body, CR may induce genotoxic, hemotoxic, neurotoxic, carcinogenic, and mutagenic effects[10]. The carcinogenicity of CR is largely associated with the formation of benzidine during its metabolic reduction[10,12], In oxygen-deficient conditions, cytochrome P450 enzymes in the liver can metabolize benzidine into reactive intermediates that covalently bind to DNA and proteins[13,7], leading to genomic instability, mutations, and eventual tumor formation, particularly in the liver and bladder[10,13] (Fig. 1). Additionally, CR may inhibit the liver enzymes aspartate aminotransferase and alanine aminotransferase, thereby impairing hepatic function. Furthermore, CR may lead to platelet aggregation and adverse effects on the skin, eyes, respiratory system, and reproductive organs[10,11]. From an environmental perspective, the presence of CR in aquatic systems can inhibit photosynthesis, increase pH, chemical oxygen demand (COD), and biological oxygen demand (BOD)[14], and disrupt the natural ecological balance of aquatic organisms. In light of these environmental challenges, the treatment of wastewater containing CR has become an urgent environmental priority. Several wastewater treatment methods, including physical, chemical, and biological approaches, have been investigated for dye removal[15]. The selection of the most effective approach depends on economic, environmental, and efficiency-related considerations. However, chemical methods may generate secondary pollutants while biological treatments often exhibit limited effectiveness. In contrast, physical methods have emerged as a major focus of research due to their high ability to remove dyes effectively

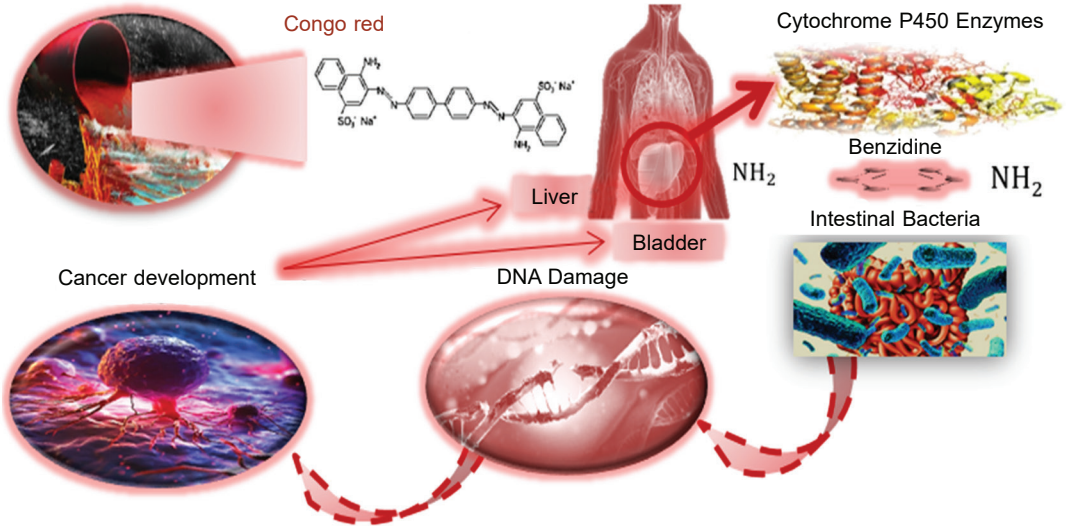

Fig. 1 – *Mutagenic potential of Congo red in wastewater and its effects on human health systems*

and are economically feasible. The adsorption process has been reorganized as one of the most effective physical treatment techniques due to its simplicity, ease of use, minimal generation of undesirable byproducts, cost-effectiveness, and high efficiency in the removal of organic and inorganic substances[16].

The valorization of agricultural waste as adsorbents for wastewater treatment offers a dual benefit by recycling these products and effectively removing organic and inorganic pollutants from wastewater. Numerous studies have focused on the application of adsorbents derived from agricultural waste, including eggshell-based materials[17], rice husk ash[18], duckweed (*Lemna* spp.)[19,20], sunflower husks[2], coconut fiber[21], tunics of corms[22], palm kernel shells[23], banana peels[24], pomegranate peels[25], *Pinus pinaster* bark[26], and *Ziziphus lotus* (ZL). In the present study, *Ziziphus lotus* stones (ZLS), a local agricultural waste derived from the fruit tree Rhamnus, locally known as Sidra, were investigated as a low-cost adsorbent. ZL is widely distributed in North Africa, including Algeria, Morocco, Libya, Tunisia, and Egypt, as well as in the Middle East, and several Southern European countries such as Greece, Cyprus, and Spain. The ZL plant has traditionally been used for medicinal purposes due to its anti-inflammatory, antioxidant, immunomodulatory, and antimicrobial properties[27]. In addition to its medicinal applications, ZL has demonstrated promising adsorption performance. Studies have reported the use of ZL leaves for removing phenol compounds[28], activated carbon derived from *Ziziphus lotus* stones for the removal of Basic Yellow 28 and Basic Red 46 dyes from aqueous media[29], the removal of cadmium using *Ziziphus Spina-Christi* leaves[30], and activated carbon synthesized from *Ziziphus* species for removal of Methylene Blue dye[31].

The novelty and significance of the present work lie in the first reported removal of the potentially carcinogenic CR dye from an aqueous solution using the kernels of the Algerian jujube tree (*Ziziphus lotus*) as a raw material without the need for additional processing steps, making it an economical and environmentally friendly absorbent. Moreover, jujube is an abundant agricultural byproduct in Algeria, and the use of advanced spectroscopy and analytical techniques, including FTIR, SEM, EDS, XRD, BET, DSC, and TGA, allows for a more precise study. In addition, Design Expert software (response surface methodology (RSM)) was employed as an effective tool to enhance absorption efficiency. The absorption mechanism was further investigated using nonlinear isotherm models such as Langmuir, Freundlich, Temkin, and Dubinin-Radushkevich, as well as nonlinear kinetic models such as pseudo-first order PFO, pseudo-second order PSO, and intraparticle diffusion IPD models, which provided more accurate statistical parameters. This research includes thermodynamic and cost analyses that provide accurate information on the economic feasibility of using this absorbent as an environmentally friendly and cost-effective alternative.

Materials and methods

Chemical reagents and instrumentation

All chemicals used in this study were of analytical grade and supplied by Sigma Aldrich. These included Congo Red dye (CR), hydrochloric acid (HCl), and sodium hydroxide (NaOH). The pH of the solutions was adjusted and measured using an Adwa AD 1000 pH meter (Romania). Adsorption experiments were conducted using a temperature-controlled rotary shaker (Nüve ST 30, Turkey), while CR concentrations were determined using a UV-visible spectrophotometer (K LAB, South Korea).

Preparation of stock dye solution

A stock solution of CR dye (1000 mg L^{-1}) was prepared by dissolving 0.5 g of CR dye powder in 500 mL of distilled water. The residual concentration of CR dye was analyzed using a UV-visible spectrophotometer, with the absorbance measured at the maximum wavelength (λ_{max}) of 498 nm. Based on the Beer-Lambert law, a concentration (C) vs. absorbance (A) calibration curve was established by correlating the absorbance with standard concentrations of CR dye prepared in the range of 1–20 mg L^{-1} with a step size of ΔC = 3 mg L^{-1} (with condition $A \leq 1$). This curve was then used to determine the unknown concentrations in the test samples.

Adsorbent preparation

Ziziphus lotus stone (ZLS) agricultural waste was collected from Laghouat, a semi-arid region in central Algeria. The collected material was thoroughly washed with tap water to remove dust and visible impurities, followed by rinsing three times with distilled water to ensure the sample high purity. The material was then boiled in deionized water for 30 min. The boiling step was considered a crucial pretreatment for removing soluble impurities and microbial content while enhancing surface activation. Subsequently, the ZLS material was oven-dried at 105 °C for 24 hours, ground using a mechanical grinder, and sieved to obtain uniform particle size fractions (100 μm). To ensure the reliability of the adsorption process using UV-visible, the ZLS powder was soaked in distilled water for 2

hours under continuous stirring, followed by oven-drying at 60 °C until a constant weight was achieved. The final product was stored in a sealed container until further use.

Instrumentation

The crystalline and amorphous nature of the ZLS adsorbent was examined using X-ray Diffraction XRD (BRUKER D8, PANalytical) with copper Kα radiation λ = 1.54060 A°. Diffractograms were collected over the 2θ range of 5.0129 to 79.9709° with a step size (2θ) of 0.026. Functional groups involved in the adsorbent-adsorbate binding were identified using Fourier transform infrared spectroscopy (FTIR-4200 JASCO, Japan) in the range of 399,1927 to 4000,6047 cm^{-1}. Nitrogen adsorption-desorption analysis, BET associated with Barrett-Joyner-Halenda BJH (ASAP 2020 plus version 2.00-Malvern Panalytical, Malvern, UK) was employed to evaluate the textural properties of the ZLS adsorbent. Scanning electron microscopy (SEM) (Thermo Scientific Prisma E) was used to observe surface morphology, while energy dispersive X-ray spectroscopy (EDS) coupled with SEM was used to determine the elemental composition. Simultaneous thermogravimetric and differential scanning calorimetry analyses (TGA/DSC) were performed using an SDT Q600 V20.9 Build 20 instrument. TGA was used to evaluate the mass loss associated with moisture evaporation, while DSC provided information regarding the endothermic and exothermic transitions associated with the adsorption process.

Adsorption experiments

Box Behnken Design for adsorption experiments

The optimization of the adsorption process was performed using response surface methodology (RSM) based on the Box Behnken Design (BBD). Three independent factors were selected: initial dye concentration (A, mg L^{-1}), solution pH (B), and adsorbent dose (C, g). The objective was to maximize CR removal efficiency. The BBD approach is a widely used statistical tool for developing second-order polynomial models for process optimization[32]. Moreover, BBD minimizes the number of required experiments while reducing experimental cost, time, and energy consumption[33,34]. In the present study, three factors (ZLS dose g, initial concentration mg L^{-1}, solution pH), at three levels (–1, 0, +1) were selected (Table 1), resulting in a total of 15 experimental runs. Three replicated center points were included to estimate pure error and improve the reliability and accuracy of the BBD matrix. Design Expert software (version 13.0.5.0) was used for statistical analyses, generation of 3D response surface plots, and 2D contour surface graphs.

Table 1 – *Experimental factors applied in the Box-Behnken design*

Factor	Codes	Unit	Levels		
			Low (–1)	Center (0)	High (+1)
Adsorbent dose	A	g	0.1	0.35	0.6
pH	B		3	5	7
Initial concentration	C	mg L^{-1}	30	65	100

The investigated experimental conditions included adsorbent doses (0.1, 0.35, and 0.6 g), solution pHs (3, 5, and 7), initial dye concentrations (30, 65, and 100 mg L^{-1}), within a constant temperature of 25 °C, a contact time of 60 min, and an agitation speed of 150 rpm. The response was the CR removal efficiency (%). The number of experimental runs (N) required in the BBD was calculated using Equation 1, while the mathematical relationship between the independent factors and the response is presented in Equation 2:

$$N = k^2 + k + C_{pt} \quad (1)$$

where: k is the number of factors, and C_{pt} is the replicate of the central points.

$$\text{Removal}(\%) = \beta_0 + \sum_{i=1}^{N}\beta_i X_i + \sum_{i=1}^{N}\beta_{ii} X_i^2 + \sum_{i<j}\sum\beta_{ij} X_i X_j + \varepsilon \quad (2)$$

The variables in the equation are defined as follows: Removal (%) is the predicted response, β_0 is the intercept term, β_i is the linear impact, β_{ii} is the cross-product impact, β_{ij} is the interaction impact, ε is the error term, and X_i is the coded factors. In statistical analysis, the relationship between the coded and uncoded values is expressed in Equation 3 as follows[31]:

$$\text{coded level} = \frac{(\text{uncoded level} - \text{mean})}{\text{half of range}} \quad (3)$$

Batch adsorption studies

Based on the BBD, the adsorption optimization experiments were conducted under controlled laboratory-scale conditions. A volume of 50 mL of CR dye solution was transferred into 125-mL flasks, which served as closed batch reactors. The experiments were performed at 25 °C using a mechanical rotatory shaker operating at 150 rpm with a contact time of 60 min, while varying the key independent

operational parameters (adsorbent dose, pH, and initial dye concentration). Following adsorption, the samples were filtered to separate the adsorbent from the solution. The equilibrium concentration of CR dye remaining in solution was determined using a UV-visible spectrophotometry (K LAB, South Korea). The CR dye removal efficiency (R/%) was calculated using Equation 4. For the adsorption isotherm studies, the effect of temperature was investigated over a range from 25 to 45 °C, while the initial dye concentration varied from 20 to 100 mg L^{-1}. These experiments were conducted under constant conditions of 60 min contact time, agitation speed of 150 rpm, pH 7, and an adsorbent dosage of 0.5 g per 50 mL of CR dye solution. The adsorption capacity at equilibrium (Q_{eq}), represented in Equation 5 [2], was used to analyze the isotherm data. In these equations, C_0, C_{eq} represent the initial and post-adsorption dye concentrations (mg L^{-1}), respectively, V_t is total solution volume, and m is the adsorbent mass (g).

$$\text{adsorption efficiency}(\%) = \left(C_o - C_{eq}\right)\cdot\left(C_0\right)^{-1}\cdot 100 \quad (4)$$

$$Q_{eq} = \left(C_0 - C_{eq}\right)\cdot(m)^{-1}\cdot V_t \quad (5)$$

Adsorption isotherm modeling

Understanding the adsorption mechanism and affinity of the adsorbent toward the target CR dye species can be achieved through adsorption isotherm studies, which describe the equilibrium relationship between the amount of adsorbate retained on the adsorbent surface and its concentration in solution. In this study, the nonlinear plots of Langmuir, Freundlich, Temkin, and Dubinin-Radushkevich (D-R) isotherms were modeled and analyzed using OriginPro Software 2026 version. The nonlinear equations for the Langmuir, Freundlich, Temkin, Dubinin-Radushkevich (D-R) isotherms are presented in Equations 6–11 [35].

$$Q_e = Q_{L-M}\cdot\frac{K_L\cdot C_e}{1+K_L\cdot C_e} \quad (6)$$

$$Q_e = K_F\cdot C_e^{\frac{1}{n}} \quad (7)$$

$$Q_e = B_T\cdot\ln\left(A_T\cdot C_e\right) \quad (8)$$

$$Q_e = Q_{D-R}\cdot\exp\left(-K_{D-R}\cdot\varepsilon^2\right) \quad (9)$$

$$\varepsilon^2 = R\cdot T\cdot\ln\left(1+\frac{1}{C_e}\right) \quad (10)$$

$$E = \frac{1}{\left(2K_{D-R}\right)^{0.5}} \quad (11)$$

where:

Q_e is the equilibrium adsorption capacity (mg g^{-1}), Q_{L-M} the maximum adsorption capacity corresponding to the adsorbate monolayer formation on the adsorbent surface (mg g^{-1}), K_L is the Langmuir constant (L mg^{-1}), C_e is the CR dye equilibrium concentration (mg L^{-1}), K_F is the Freundlich constant ((mg g^{-1})(L $mg^{-1})^{-1/n}$), 1/n is the dimensionless Freundlich constant indicating the adsorption intensity and heterogeneity factor, B_T is the Temkin constant related to adsorption heat (J mol^{-1}), A_T is the Temkin isotherm equilibrium binding constant indicating the binding affinity of the adsorbent for the adsorbate (L g^{-1}), Q_{D-R} is the Dubidin-Radushkevich maximum adsorption capacity (mg g^{-1}), K_{D-R} is the constant related to adsorption energy (mol^2 kJ^{-2}), ε is Polanyi potential indicating the potential energy change when transferring a molecule from the bulk solution to the surface (J mol^{-1}), R is the universal gas constant (8.314 J mol^{-1} K^{-1}), T is the absolute temperature (K), E is the mean free energy of adsorption (E < 8 kJ mol^{-1}, physisorption and 8 < E < 16 kJ mol^{-1}, chemisorption).

Adsorption kinetics study

To achieve a more deeper understanding of the adsorption mechanism and identify the rate-controlling step (chemical or physical), the experimental kinetic data were analyzed using three established kinetic models: the pseudo-first-order (PFO), pseudo-second-order (PSO), and intraparticle diffusion (IPD) models. The mathematical expressions of these models are given as follows: Equation 12 [36], Equation 13 [37], and Equation 14 [38], respectively.

$$Q_t = Q_e\left(1-e^{-K_1 t}\right) \quad (12)$$

$$Q_t = \frac{Q_e^2\,K_2\,t}{1+Q_e K_2 t} \quad (13)$$

$$Q_t = K_{ID}\,t^{1/2} + C \quad (14)$$

where:

Q_e and Q_t (mg g^{-1}) represent the adsorption capacities at equilibrium and at time t, respectively. K_1 (min^{-1}) and K_2 (g mg^{-1} min^{-1}) are the rate constants of the PFO and PSO models, respectively. K_{ID} (mg g^{-1} $min^{-1/2}$) is the intraparticle diffusion rate constant, and C is a constant related to the boundary layer thickness.

Adsorption thermodynamic studies

The main thermodynamic parameters, namely Gibbs free energy (ΔG^0), enthalpy (ΔH^0), and entropy (ΔS^0), were determined using Equation 15. The values of ΔH^0 and ΔS^0 were determined from the slope and intercept of the Van't Hoff plot of ln K_C

versus $1/T$, according to Equations 16 and 17 [39], respectively.

$$\Delta G^0 = \Delta H^0 - T\Delta S^0 \quad (15)$$

$$K_C = \frac{C_S}{C_e} \quad (16)$$

$$\ln K_C = -\frac{\Delta H^0}{R}\cdot\frac{1}{T} + \frac{\Delta S^0}{R} \quad (17)$$

where:

K_C is the equilibrium constant, C_S is the equilibrium concentration of the dye in the solid phase (mg L^{-1}), and C_e represents the equilibrium concentration of the liquid phase.

Results and discussion

Characterization

X-ray Diffraction (XRD) analysis

The patterns and smoothed curves of X-ray diffraction XRD analysis, as shown in Fig. 2, provided the structural features observed in the ZLS sample. Peaks at 15.022° and 22.27° correspond, respectively, to the semi-crystalline plane index (1 0 1) and the crystal plane (0 0 2) of the cellulose structure[40]. Furthermore, the absence of γ-bands associated with amorphous and aliphatic structures is indicated by the high symmetry of (0 0 2). The crystallinity index (C_fI) and the crystallinity rate (C_r/%) of ZLS were determined to be 59.7239 % and 0.7394, respectively, employing the Segal method presented in the following equations[40,41]:

$$C_fI = \frac{\left(I_{maxC} - I_{maxA}\right)}{I_{maxC}} \quad (18)$$

$$C_r(\%) = \frac{I_{maxC}}{\left(I_{maxC} - I_{maxA}\right)}\cdot 100 \quad (19)$$

where I_{maxC} and I_{maxA} represent, respectively, the maximum intensity of the amorphous phase and the maximum intensity of the crystalline phase. These results reflect a partially ordered structure.

Regarding the diffraction peaks, 34.75693° and 38.21493° were attributed to residual inorganic impurities present in the ZLS structure and confirmed by EDS analysis.

Surface morphology and elemental analysis (SEM-EDS)

The morphological characteristics of ZLS before and after adsorption are presented in Fig. 3 (a, b, c, and d), respectively. The surface features were examined at different levels of magnification (50, 100, and 500 μm). In general, ZLS particles exhibited an oval shape with a heterogeneous and rough surface morphology, nonuniform pore distribution, and interconnected mesopores and micropores. Surface cracks are advantageous for the adsorption process because they enhance the accessibility of the adsorbate to the active adsorption sites. As shown in Fig. 3d, the SEM micrograph after adsorption revealed noticeable filling of surface pores, as well as the formation of deposits on the surface, indicating the successful adsorption of CR dye molecules.

Table 2 – *Elemental composition of the ZLS adsorbent determined by EDS analysis*

(a)

Chemical species	Weight/%	Atomic/%
C	59.11	65.92
O	40.45	33.86
Al	0.44	0.22

(b)

Chemical species	Weight/%	Atomic/%
C	82.10	87.34
O	15.32	12.26
Mg	0.22	0.12
Mo	2.36	0.31

Complementary elemental analysis of ZLS before and after the adsorption process was performed using energy-dispersive X-ray spectroscopy (EDS), and the corresponding spectra are presented in Fig. 3(e-f) and Table 2 (a-b). The organic nature of ZLS was confirmed by the EDS spectrum through the dominant peaks of carbon and oxygen, with atomic 65.92 % and 33.86 %, respectively. In addition, the low background noise observed in the spectrum demonstrated the reliability of the measurements. Trace amounts of aluminum (0.22 % atomic) were also detected. After adsorption, a notable increase in the carbon atomic from 65.92 % to 87.34 % and a decrease in oxygen atomic from 33.86 % to 12.23 % were observed. These changes were attributed to the adsorption of Congo Red molecules, which possess high carbon content, while the deposited dye layer partially masked oxygen-containing functional groups, resulting in a reduced oxygen signal. These findings confirm the successful adsorption of CR dye onto ZLS.

Fourier transform infrared spectroscopy FTIR

The FTIR spectra presented in Fig. 4 provided the information regarding the functional groups present on ZLS before and after CR dye adsorption based on the intensity and position of stretching vibrations. Furthermore, FTIR analysis defined the chemical bonds that contributed to the adsorption

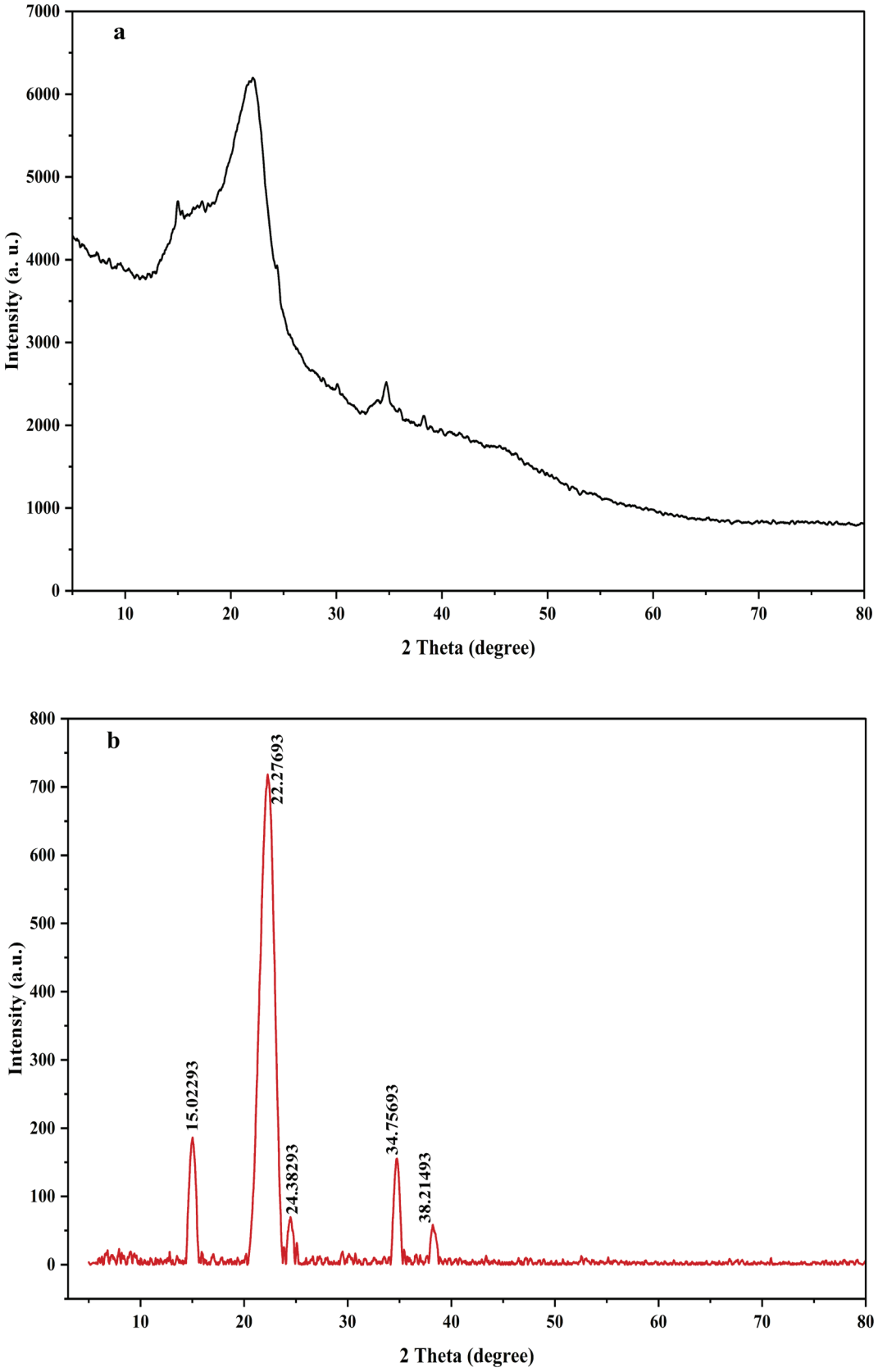

Fig. 2 – *(a) XRD pattern, and (b) smoothed ZLS adsorbent profile*

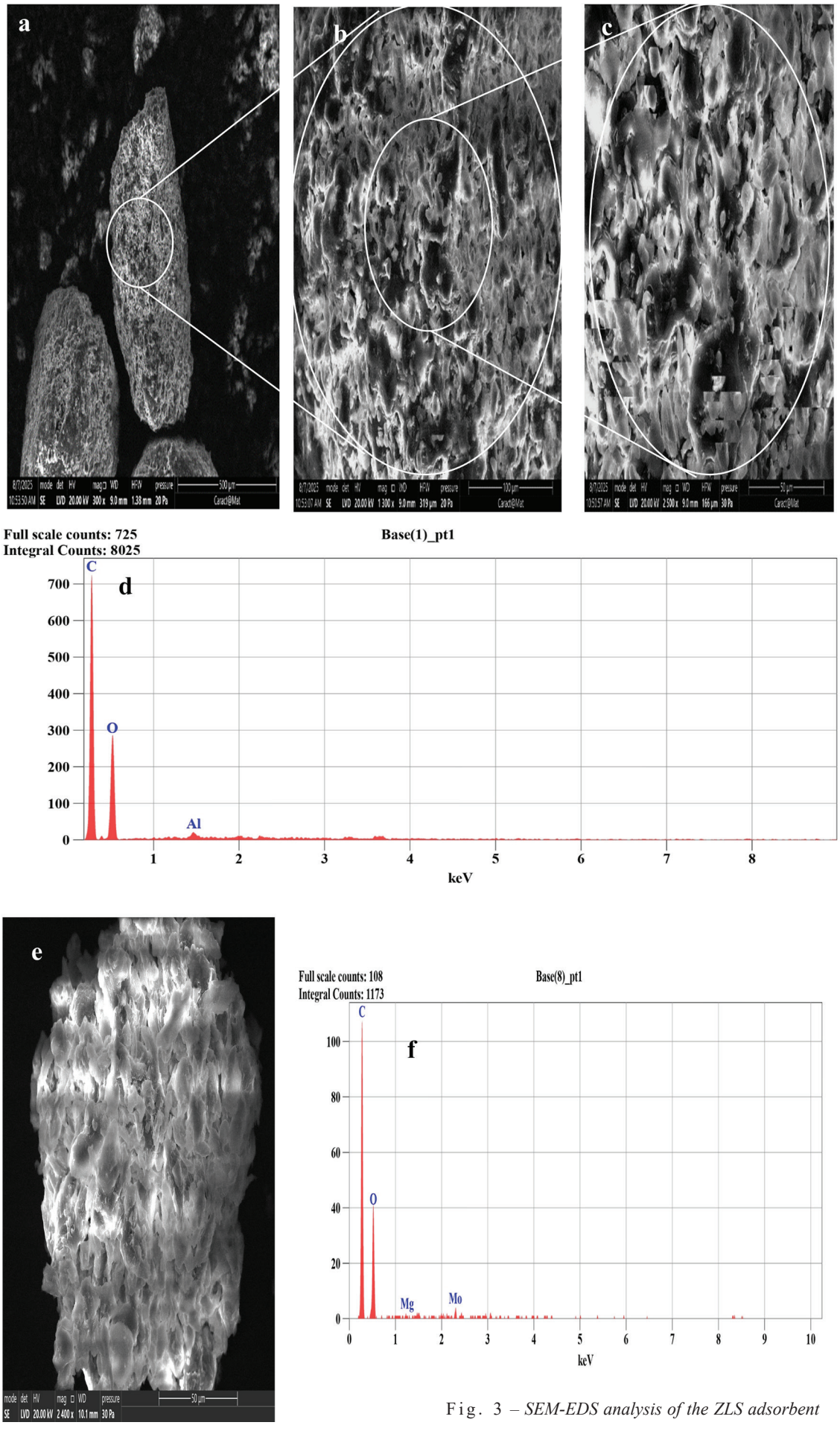

Fig. 3 – *SEM-EDS analysis of the ZLS adsorbent*

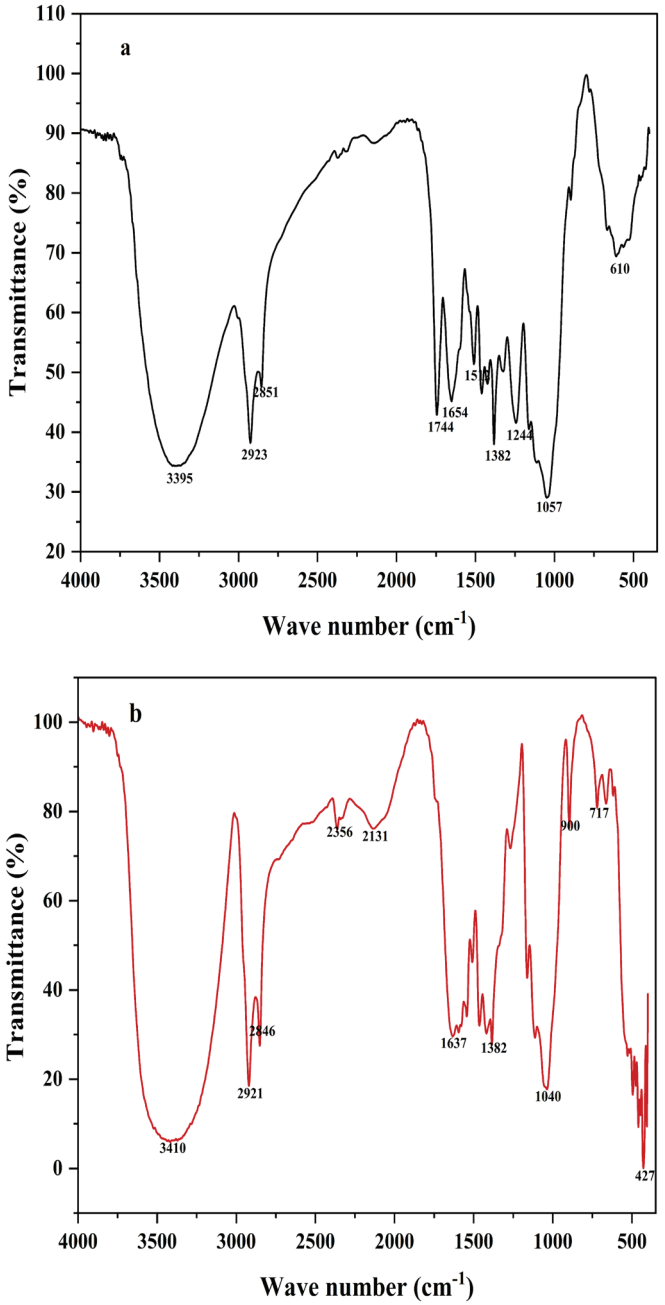

Fig. 4 – *FTIR spectra of the ZLS adsorbent before and after adsorption of Congo red (CR) dye*

process. Before adsorption, a broad and intense band centered around 3395 cm^{-1} was attributed to stretching of (–OH) associated with hydroxyl groups present in alcohols or phenol. These OH groups also indicate the presence of hydrogen bonds in the intermolecular and intranetwork within the cellulose matrix. Peaks in the 2923–2851 cm^{-1} range were assigned to cellulose aliphatic saturated (C–H) stretching[42]. The peak at 1744 cm^{-1} corresponds to (C=O) conjugated stretching vibrations associated with carboxylic or ester functional groups typically present in pectin and hemicellulose structures[43]. Peaks located between 1654 and 1513 cm^{-1} were attributed to C=C stretching vibrations in aromatic or conjugated systems related to lignin biomaterials[44]. Within the fingerprint region (1500–500 cm^{-1}), the peaks at 1382, 1244, 1057, and 610 cm^{-1} were associated with C–H bending and/or O–H deformation[45], asymmetric C–O–C stretching characteristic of ether linkage in hemicellulose and pectin[46], C–O stretching vibrations found in cellulose glycosidic linkages[43], and C–H out-of-plane bending vibration of aromatic rings potentially originating from lignin[47], respectively. After adsorption, significant modifications in the FTIR spectrum were observed, indicating interactions between the adsorbent and CR dye molecules. An increase in the absorbance intensity of the –OH bond suggests the participation of this function in the adsorption process. Weak peaks and bands appearing at 2364–2129 cm^{-1} may correspond to vibrational modes (N=N) or (C=N), indicating possible azo-related rearrangements and the emergence of nitrile or alkyne functionalities[44], which are not dominant but show faint chemical interactions at the adsorbent-dye interface. The disappearance and shifting of peaks within the 1744–1513 cm^{-1} region suggest the direct involvement of ester carbonyl (C=O) and aromatic (C=C) groups in the interaction with CR dye, likely through taking part in surface-level chemical changes such as π-π stacking or hydrogen bonding[7]. A low-intensity peak observed at 1264 cm^{-1} ascribed either to (C–O) stretching vibrations of sulfonate (SO_3^-) groups in CR dye, raising the possibility of ionic interactions between the positively charged ZLS surface and the negatively charged sulfonate groups, or to (C–N) stretching in aromatic compounds. Similar findings have been reported in the previous studies[48]. The presence of an intense low-frequency peak at around 425 cm^{-1} was attributed to mineral-oxygen stretching vibrations on the adsorbent surface and the sulfonate moieties of the CR dye, enhancing the participation of inorganic components in the adsorption process[49].

BET/BJH analysis of ZLS texture

Brunauer-Emmet-Teller (BET) analysis combined with the Barrett-Joyner Halenda (BJH) method provided information regarding the textural properties of the ZLS adsorbent. Fig. 5a shows the N_2 adsorption-desorption isotherms obtained at 77 K. According to the IUPAC classification, the isotherm corresponds to a type IV profile with an H3-hysteresis loop, confirming the mesoporous nature of the material[50]. Mesoporous materials are characterized by pore sizes in the range 2–50 nm [51]. The specific surface area (S_{BET}), total pore volume (V_{total}), and pore size values of ZLS were determine to be 4.7758 $m^2\ g^{-1}$, 0.001736 $cm^3\ g^{-1}$, and 4.3578 nm, respectively. The obtained S_{BET} value falls within

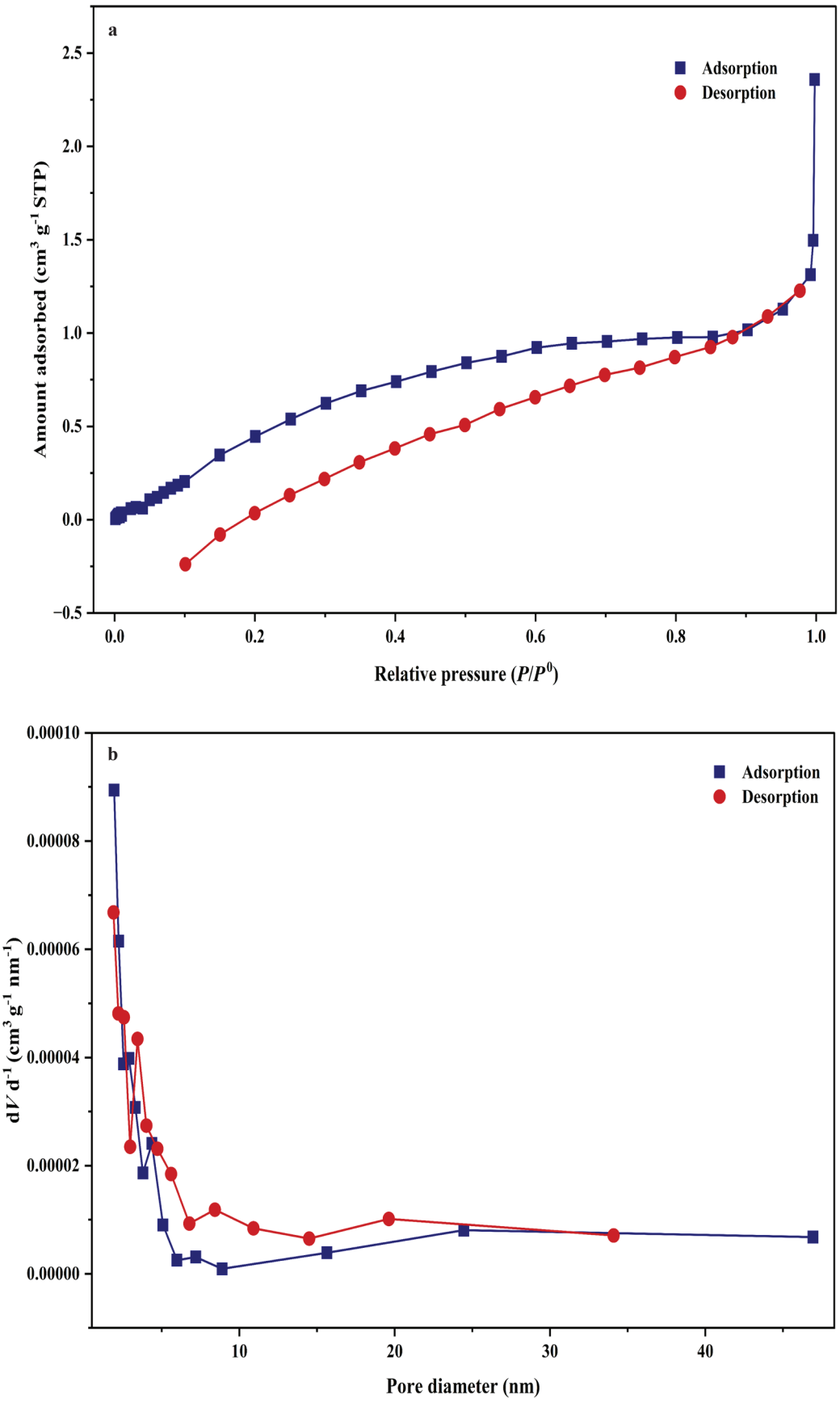

Fig. 5 – *(a) N_2 adsorption-desorption isotherms and BET analysis, and (b) pore size distribution and BJH curves of the ZLS adsorbent*

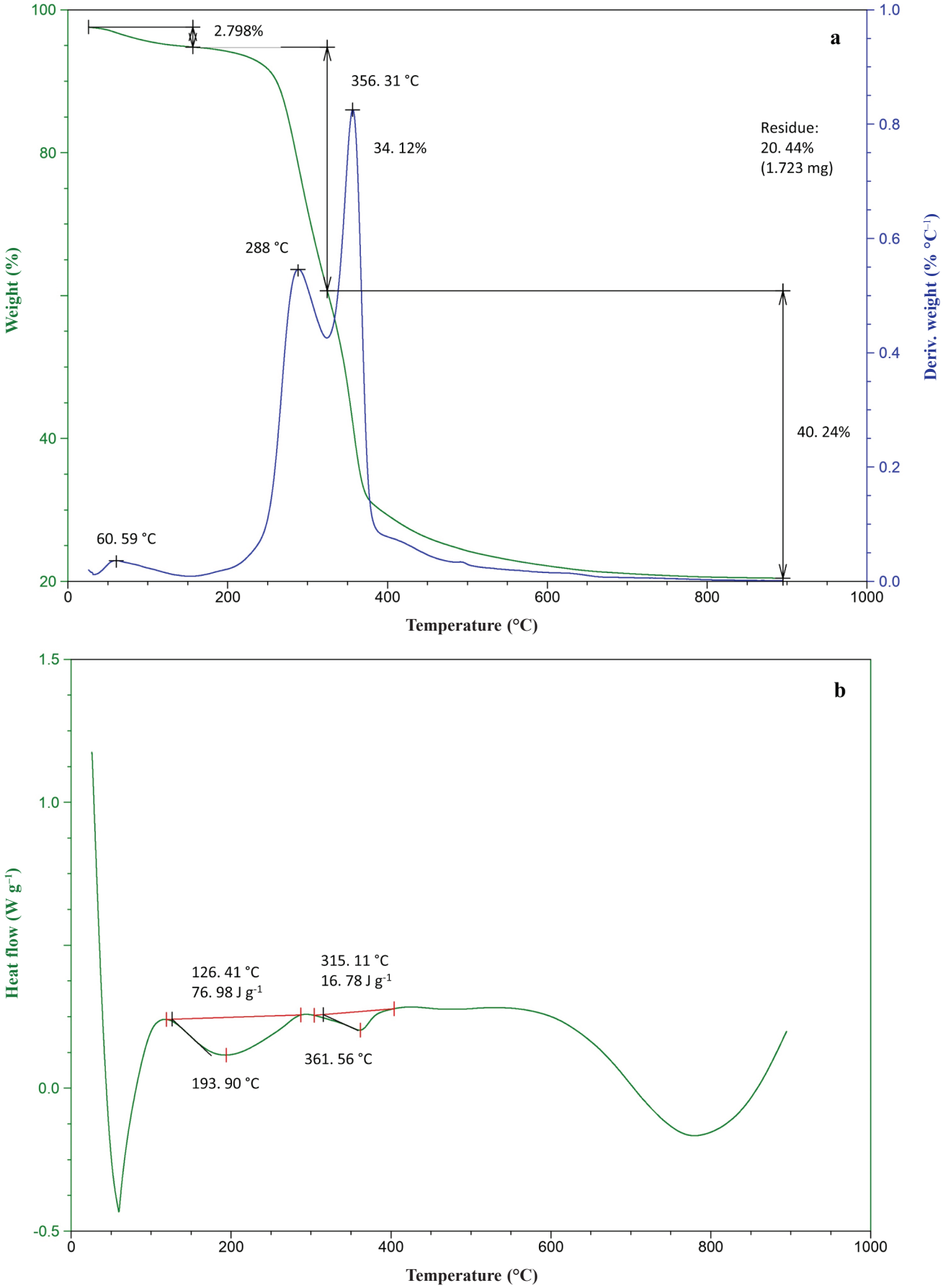

Fig. 6 – *(a) TGA/DTG curves of the ZLS adsorbent, and (b) DSC thermogram of the ZLS adsorbent*

the expected range for untreated lignocellulosic materials. At low relative pressure (P/P^0), the adsorption isotherm exhibited gradual uptake, followed by a sharp increase at higher relative pressure, indicating capillary condensation within the pore network. The open hysteresis loop observed upon desorption was explained by the expansion of the nonrigid slit-shaped pores and interconnected porous structures.

Thermal behavior and stability analysis (TGA/DTG-DSC)

Fig. 6a provides a thermoanalytical profile for the evaluation of ZLS adsorbent using (TGA/DTG-DSC) analysis. The curves reveal three major transitions in response to temperature increase, associated with moisture, cellulose, hemicellulose, and lignin components present in ZLS. Within the low-temperature range 26–170 °C, TGA analysis indicated about 2.8 % total mass loss, accompanied by a sharp DTG peak and an endothermic DSC peak at ~59 °C, reflecting the evaporation of physically bound moisture entrapped within the porous structure[52].

In the moderate thermal region 170–370 °C, TGA displays a marked decline of 34 % in mass loss. At the same time, the DSC (Fig. 6b) displayed two successive endothermic signals with enthalpy changes of 76.98 and 16.78 J g^{-1}, respectively, corresponding to the rapid decomposition of cellulose and hemicellulose[53]. According to the DTG analysis and previous literature reports, hemicellulose decomposed at 288 °C, whereas cellulose, as a semi-crystalline β-1, 4-linked glucan, degraded at 356 °C [54]. The DTG analysis proved particularly valuable for accurately identifying the decomposition temperatures of the hemicellulose and cellulose components of the ZLS adsorbent. At higher temperatures (370–900 °C), the TGA/DTG curves showed a nearly stable baseline at ~20 % residual mass. The DSC displayed a broad signal at ~780 °C, indicating the gradual thermal decomposition of lignin[52,53]. Lignin showed a high temperature resistance due to its high molecular weight as an amorphous, cross-linked aromatic polymer[55]. The synergetic application of TGA/DTG and DSC analyses provided a multidimensional thermal profile of the ZLS adsorbent.

pH determination at the point of zero charge (pHpzc)

Fig. 7 illustrates the variation of (pH_i-pH_f) as a function of the initial pH (pH_i) for the ZLS adsorbent. The point of zero charge (pH_{pzc}) is found where the curve crosses the baseline pH_i, demonstrating no change in pH. For the ZLS adsorbent, the pH_{pzc} value was found to be 5.75. When pH>5.7, the adsorbent surface becomes negatively charged due to deprotonation[56].

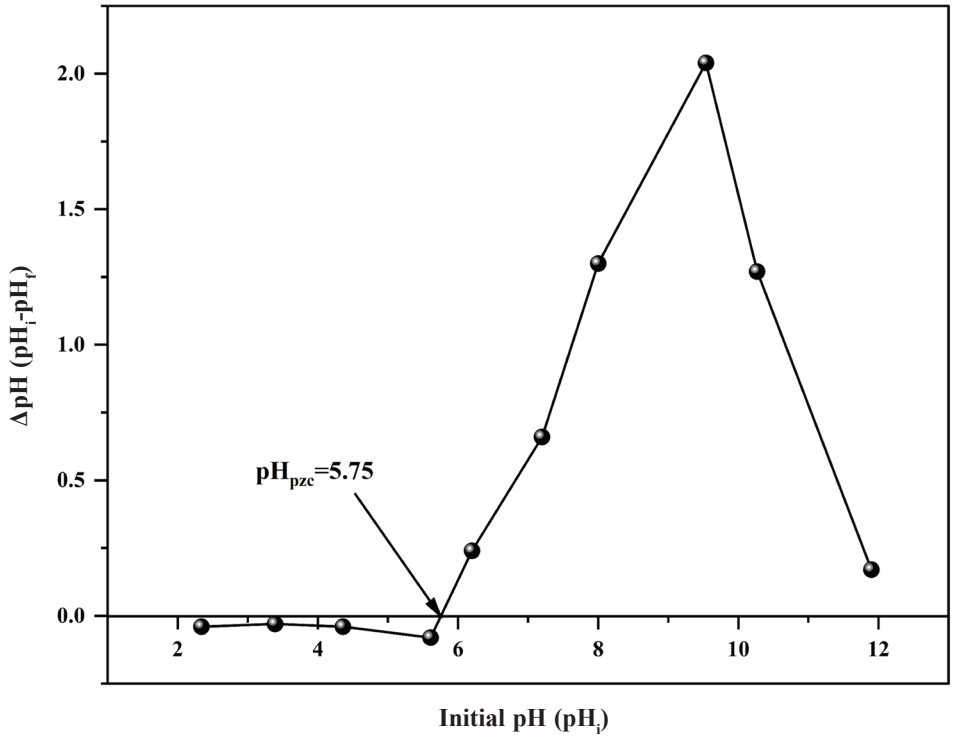

Fig. 7 – *pH_{pzc} of the ZLS adsorbent (T = 25 °C, 150 rpm, 24 h)*

BBD evaluation and validation

Using Design Expert software (version 13.0.5.0), the experimental setup for the adsorption process was generated computationally within 56 ms using the BBD matrix. Based on the statistical summary and analysis of variance (ANOVA), the quadratic design model was selected because the difference between the predicted R^2 and the adjusted R^2 values was less than 0.2, indicating reasonable agreement between the experimental and predicted data. In this study, the coefficient of determination values were $R^2 = 0.9882$, adjusted $R^2 = 0.9670$, and predicted $R^2 = 0.8177$. A p-value < 0.05 confirmed model reliability. Furthermore, the lack-of-fit test was insignificant ($p = 0.0571 > 0.05$), confirming the adequacy of the selected model.

Table 3 – *Experimental and model-predicted responses obtained from the BBD design*

RUN	Factors (Input)			Response (output)	
	Initial concentration	pH	Adsorbent dose	Experimental removal	Predicted removal
	mg L^{-1}		G	%	
1	1	–1	0	47.8008	48.0488
2	1	1	0	86.6158	88.0459
3	0	–1	–1	40.4	38.9295
4	–1	–1	0	77.9412	76.5097
5	1	0	–1	45.648	46.8671
6	–1	1	0	85.4545	85.2050
7	–1	0	1	86.0123	84.7918
8	1	0	1	75.6164	72.7137
9	0	1	–1	54.4327	51.7804
10	0	1	1	86.9208	88.3903
11	–1	0	–1	57.5078	60.4091
12	0	–1	1	49.8976	52.5489

The ANOVA results presented in Table 4, demonstrated that the interaction between initial concentration, pH, and pH-adsorbent dose is a significant factor. Moreover, the quadratic impacts of initial concentration and adsorbent dose were significant at a p-value lower than 0.05 for the four mentioned terms.

The lack-of-fit F-value of 16.69 ($p = 0.0571$) indicates a 5.71 % probability that deviations in the model resulted from random noise. This relatively low probability (<10 %) is troubling. The model F-value of 46.60 demonstrates its high statistical significance, with only a 0.03 % probability that an F-value this high could result from random noise.

The relationship between CR removal efficiency % and the three factors — A: initial concentration (mg L^{-1}), B: pH, and C: ZLS dose (g) — is described by the regression Equations (20) and (21), which represent the terms of the coded and actual factors, respectively. The predicted removal efficiencies are presented in Table 3.

Table 4 – *ANOVA results for the removal efficiency of CR dye*

Source	Sum of squares	Mean square	Degrees of freedom	F-value	p-value	
Model	3700.76	411.20	9	46.60	0.0003	Significant
A-Initial concentration	328.12	328.12	1	37.19	0.0017	
B-pH	1185.46	1185.46	1	134.35	< 0.0001	
C-Adsorbent dose	1261.49	1261.49	1	142.97	< 0.0001	
AB	244.95	244.95	1	27.76	0.0033	
AC	0.5358	0.5358	1	0.0607	0.8151	
BC	132.14	132.14	1	14.98	0.0118	
A^2	271.74	271.74	1	30.80	0.0026	
B^2	0.3225	0.3225	1	0.0366	0.8559	
C^2	234.03	234.03	1	26.52	0.0036	
Residual	44.12	8.82	5			
Lack of Fit	42.42	14.14	3	16.69	0.0571	Not Significant
Pure Error	1.69	0.8473	2			
Cor Total	3744.88		14			

$$\text{Removal (\%)} = 65.58 - 6.40\,A + 12.17\,B + 12.56\,C + 8.58\,A^2 + 0.2956\,B^2 - 7.96\,C^2 + 7.83\,AB + 0.3660\,AC + 5.75\,BC \quad (20)$$

$$\text{Removal (\%)} = 102.69136 - 1.66699\ \text{initial concentration} - 5.94216\ \text{pH} + 79.20214\ \text{adsorbent dose} + 0.007003\ (\text{initial concentration})^2 + 0.073888\ (\text{pH})^2 - 127.38280\ (\text{adsorbent dose})^2 + 0.111792\ (\text{initial concentration})\ (\text{pH}) + 0.041828\ (\text{initial concentration})\ (\text{adsorbent dose}) + 11.49527\ (\text{pH})\ (\text{adsorbent dose}) \quad (21)$$

The influence of each independent factor on the CR removal efficiency (%) was analyzed based on the deviation from the reference point (0 on coded unit), as presented in Fig. 8a. The linear trend associated with factor B indicated a proportional effect of pH on the removal efficiency, whereas factors A and C exhibited quadratic behavior, suggesting the existence of optimal values for the initial concentration and adsorbent dose for maximum removal efficiency. The steep slope of the initial concentration factor highlights its strong influence on CR removal efficiency. Fig. 8b compares the predicted and experimental CR removal efficiencies. The close alignment of the data points with the diagonal line forced the BBD model accuracy and confirmed its reliability for predicting CR removal efficiency (%). Further analysis is presented in Figs. 8c–8e, which represent the interaction of the factors (AB, AC, and BC). Significant interactions were observed between AB and BC, whereas the AC interaction was statistically insignificant.

3D/2D visualization of the factor interaction effect on the CR removal efficiency

The 3D response surface plots and the corresponding 2D contour plots are presented in Figs. 9a–9f. These plots were generated by simultaneously varying two parameters while maintaining the third at the central level, resulting in a partial parabolic cylinder. The final surface plots exhibited distinct maxima and minima within the visible range, thereby highlighting the combined effect of the independent factors on the CR removal efficiency.

Combined effect of initial concentration and pH

Figs. 9a–9b represent the variation in CR removal efficiency as a function of the initial dye concentration and solution pH at a fixed adsorbent dose corresponding to the center level. The CR removal efficiency increased significantly from 40 % to more than 86 % as the pH increased from acidic conditions to pH 6–7. Within this pH range, maximum removal efficiencies were obtained at both low and high dye concentrations (30 and 100 mg L^{-1}). This finding demonstrates the critical role of pH in the adsorption process. The improved adsorption performance at pH 7 is related to both the pKa value of CR dye and the pH_{pzc} value of the ZLS adsorbent. The ZLS surface becomes positively charged when $pH<pH_{pzc}$ and negatively charged when $pH>pH_{pzc}$ [5]. In contrast, the degree of ionization of the CR solution is influenced by its pKa value (4.1) [57]. At pH values below the pKa, CR predominantly exists in its protonated form[58]. In this state, the dye retains protons on its amine groups (NH_2/–NH), which often become $–NH^+_3$ or $–NH^+_2$, –OH, and $–SO_3H$ [7]. This protonated form in an acidic medium may also induce a color change from red to blue ($pH \leq 3$)[58]. The pH of the ZLS adsorbent was determined to be 5.75, implying that for pH below 5.75, the surface of ZLS is positively charged. CR existed primarily in its protonated form within the pH range of 3–4.1. Consequently, the electrostatic interaction between the protonated CR and the positively charged surface was moderate or relatively weak. Within the pH range of 4.1 – 5.75, the CR solution exhibited dominant deprotonated form; this charge difference facilitated electrostatic interactions among the charged species, leading to the enhancement of adsorption performance. At pH = 5.75, the adsorbent became electrically neutral, reducing it affinity toward negatively charged CR molecules. The maximum adsorption efficiency was observed at the native CR solution pH of 7, despite both the ZLS surface ($pH>pH_{pzc}$) and CR solution (pH>pKa) being negatively charged. This indicated that adsorption under these conditions was not governed primarily by electrostatic attraction, but rather that adsorption occurred through additional interactions such as hydrogen bonding, van der Waals forces, π–π stacking between the aromatic rings of CR and lignin aromatic structures in ZLS, and specific surface binding interactions[26]. Therefore, pH 7 represents an optimal operational condition because it provided high CR removal efficiency while minimizing the need for pH adjustment, thereby reducing overall process cost.

At low CR initial concentrations and $pH>pH_{pzc}$, the positive effect on adsorption efficiency can be attributed to the abundance of available adsorption sites relative to the number of dye molecules[15]. Similar behavior was also observed at high initial concentrations due to the ZLS surface area being saturated with CR molecules. Despite the potential for electrostatic repulsion between the negatively charged ZLS surface and the CR solution, the persistence of adsorption further confirmed the contribution of nonelectrostatic interactions, including hydrogen bonding and Van der Waals forces. These

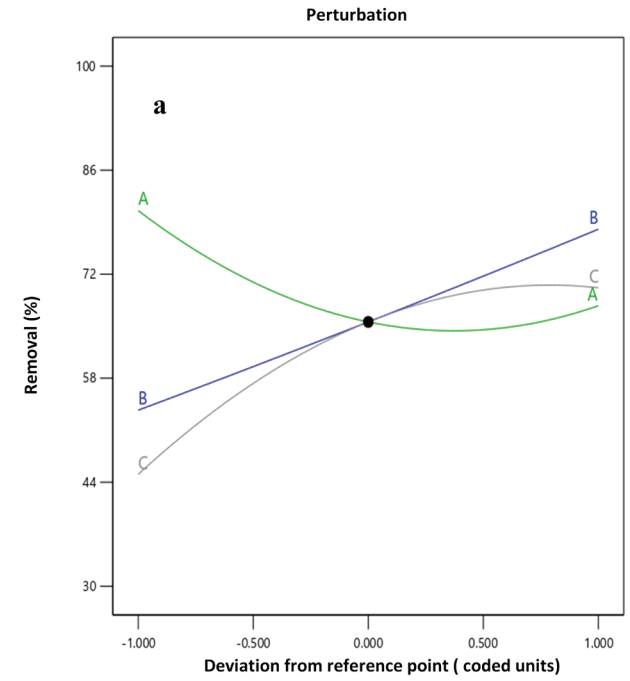

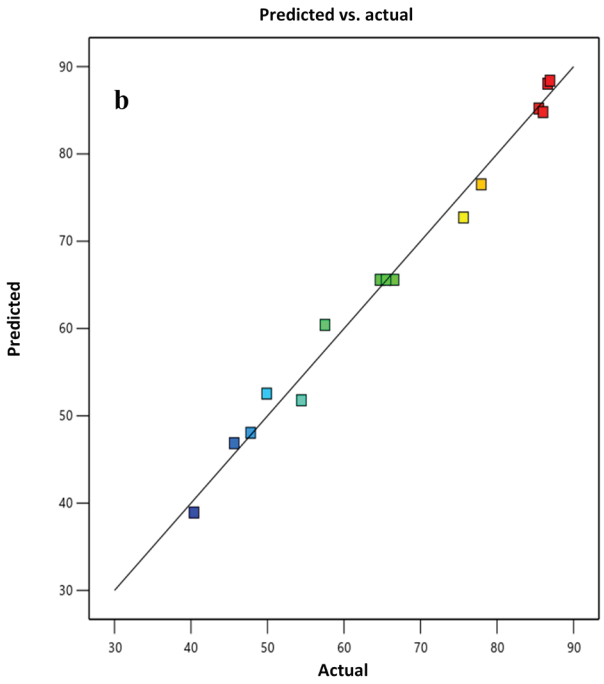

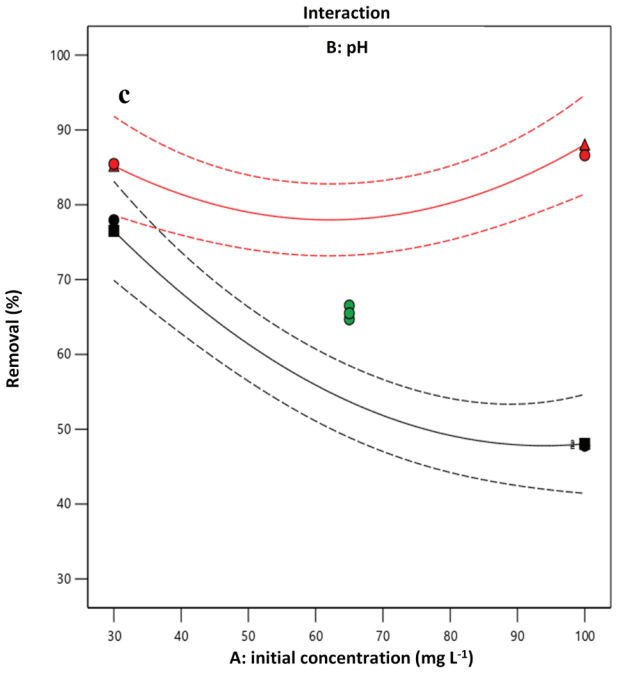

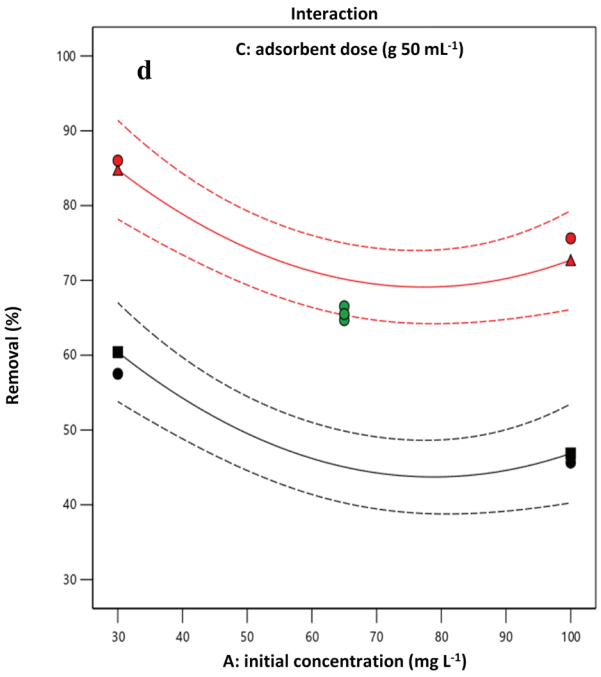

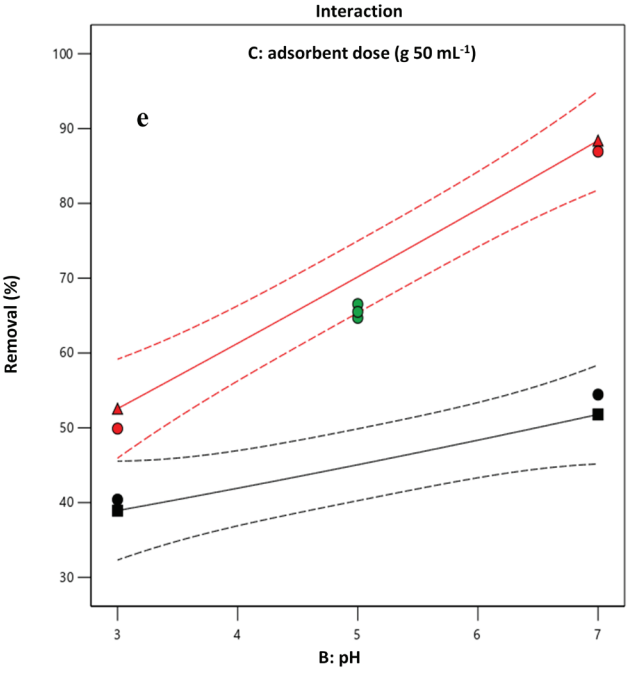

Fig. 8 – *(a) Deviation from the reference point (coded unit) versus removal %; (b) actual versus predicted responses; (c) interaction plots pH-initial concentration; (d) interaction plots of adsorbent dose-initial concentration, (e) interaction plots of pH-adsorbent dose*

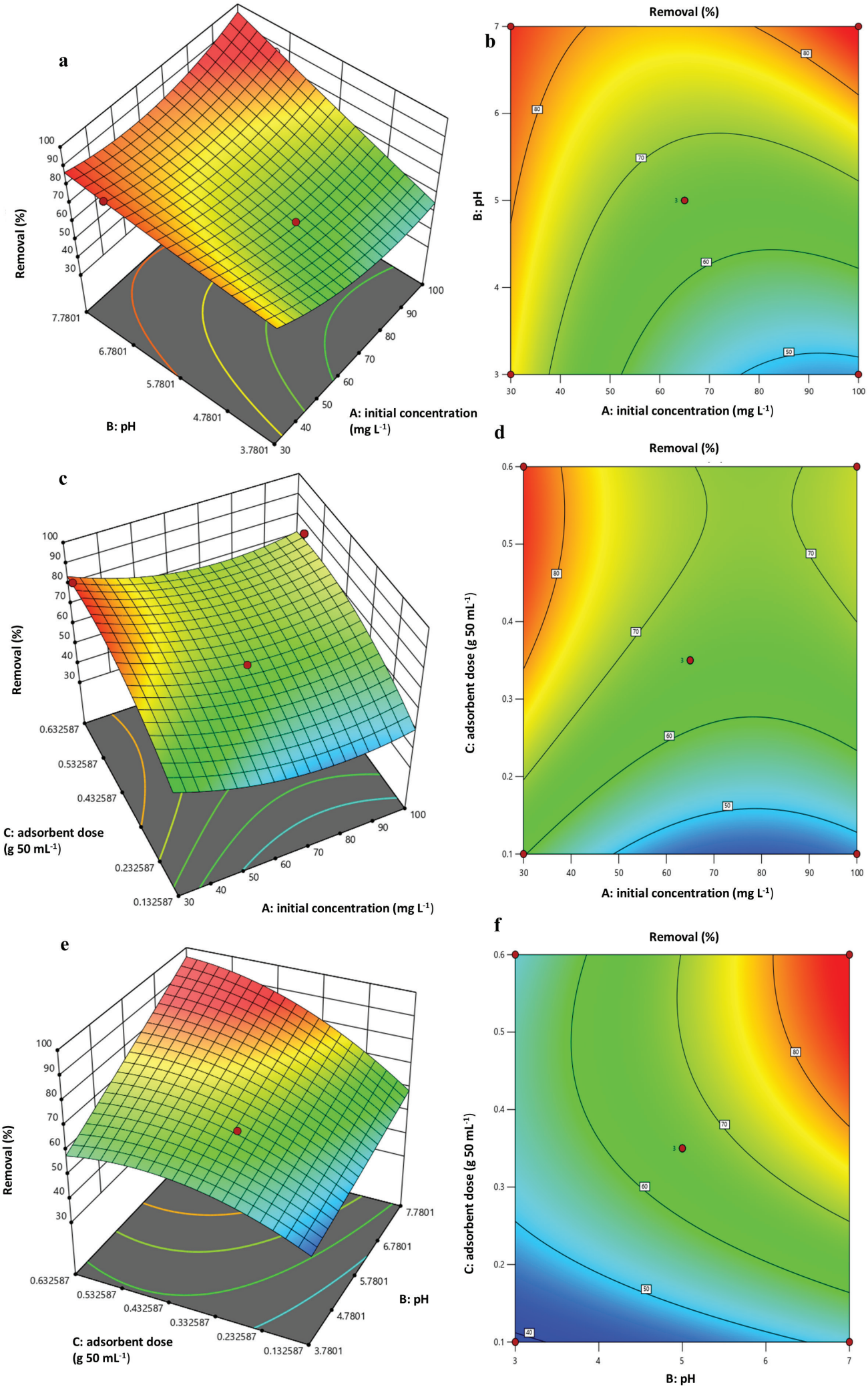

Fig. 9 – *3D/2D plots of the factors influencing CR % dye removal %, (a, b) pH-initial concentration, (c, d) adsorbent dose-initial concentration, and (e, f) pH-adsorbent dose*

findings indicate that both electrostatic and non-electrostatic mechanisms synergistically contributed to the adsorption process at pH 7.

Combined effect of initial concentration and ZLS dose

Figs. 9c–9d present the variation in CR removal efficiency as a function of initial dye concentration and adsorbent dose while maintaining the pH at its center value. The adsorption efficiency increased proportionally with increasing ZLS dosage, particularly at lower CR concentrations. These findings can be explained by the fact that, at pH ~ pH_{pzc}, electrostatic interaction between adsorbent and adsorbate was limited, and the adsorption process was primarily controlled by the abundant sites on the ZLS surface[11]. At low dye concentrations, the increase in removal efficiency became less pronounced because the limited number of dye molecules effectively utilized the available adsorption sites.

Combined effect of pH and ZLS dose

Figs. 9e–9f illustrate the combined influence of pH and adsorbent dose on CR removal efficiency while maintaining the initial dye concentration at its center level. The removal efficiency increased proportionally with increasing pH within the range of 6–7, while the ZLS dose exhibited the same positive effect on CR removal. A significant enhancement in removal efficiency, from 40 % to 86 %, was achieved by increasing the adsorbent dose. The increased availability of binding sites promoted stronger adsorbent–adsorbate interactions, thereby enhancing CR removal efficiency. However, for a 0.4 g ZLS dose, the removal efficiency reached a plateau due to the saturation of active sites, and the number of available sites exceeding the number of dye molecules present in solution. Similar findings have been reported in previous studies[7].

Optimization analysis of CR dye adsorption using BBD

The optimum conditions (initial concentration, pH, and adsorbent dose) for maximizing CR removal efficiency were predicted using the BBD model. Numerical optimization and probabilistic analysis for the response were performed using Design Expert software (version 13.0.5.0), assigning the following inputs as goals: none, maximize, minimize, within range, and target. The factors were adjusted to maximize, minimize, target, equal to, and within range. The optimum conditions were determined by maximizing the goal of both the factors and the response. Seven possible solutions were identified, and the selected solution is represented in a 2D contour plot (Fig. 10), for an extremely promising 96.384 % of CR removal with CR concentration of 100 mg L^{-1}, adsorbent dosage of 0.5 g, and solution pH of 7 (Fig. 10). Experimental validation under the optimized conditions yielded a removal efficiency of 95.2 %, confirming both the reliability of the BBD model and the high adsorption capability of the ZLS adsorbent for highly concentrated CR solutions. A 10 % process optimization was achieved with a minimum number of experiments.

Investigation of temperature influence and adsorption isotherm behavior for CR removal

To achieve a deeper understanding of the adsorption mechanism and the nature of the adsorbent-adsorbate interactions established at equilibrium, adsorption isotherms and the effect of temperature on CR removal efficiency (%) were investigated, as illustrated in Figs. 11a–e. The 3D bar graph in Fig. 11e shows the effects of temperature (25, 35, and 45 °C) on the CR removal efficiency at different initial concentrations ranging from 20 to 100 mg L^{-1}. The results indicate that the effect of temperature on CR removal performance depended on the initial dye concentration. At low concentrations, the active sites on the ZLS surface are abundantly available, minimizing the need for additional thermal energy, as the CR dye molecules can readily occupy the active sites on the ZLS surface. At moderate concentrations, however, the adsorption sites on the ZLS surface begin to approach saturation at 25 °C. Increasing the temperature enhances both the kinetic energy and diffusivity of CR dye molecules, thereby improving access to additional adsorption sites. At high concentrations, the effect of temperature becomes less significant, as a quasi-equilibrium state is established between the available adsorption sites and the excess CR dye molecules. Overall, 25 °C can be considered the most suitable adsorption temperature, since high removal efficiencies, ranging from 91 to 98 % were achieved for CR concentrations between 100 to 20 mg L^{-1}, respectively. This observation indicates that the adsorption process was exothermic in nature[2,26]. Fig. 11a–d presents the experimental nonlinear isotherm curves of the Langmuir, Freundlich, Dubinin-Radushkevich (D-R), and Temkin models obtained at 25, 35, and 45 °C, while Table 5 summarizes the corresponding model parameters. The results reveal that the Freundlich isotherm (Fig. 11b) most appropriately describes the adsorption system under the investigated conditions. This conclusion is supported by the better fit and the high regression coefficients (R^2 0.95, 0.989, and 0.987), and the low reduced χ^2 values (0.552, 0.116, and 0.142) obtaines at 25, 35, and 45 °C, respectively. These findings confirm the heterogeneous and non-uniform nature of the ZLS surface and reflect the

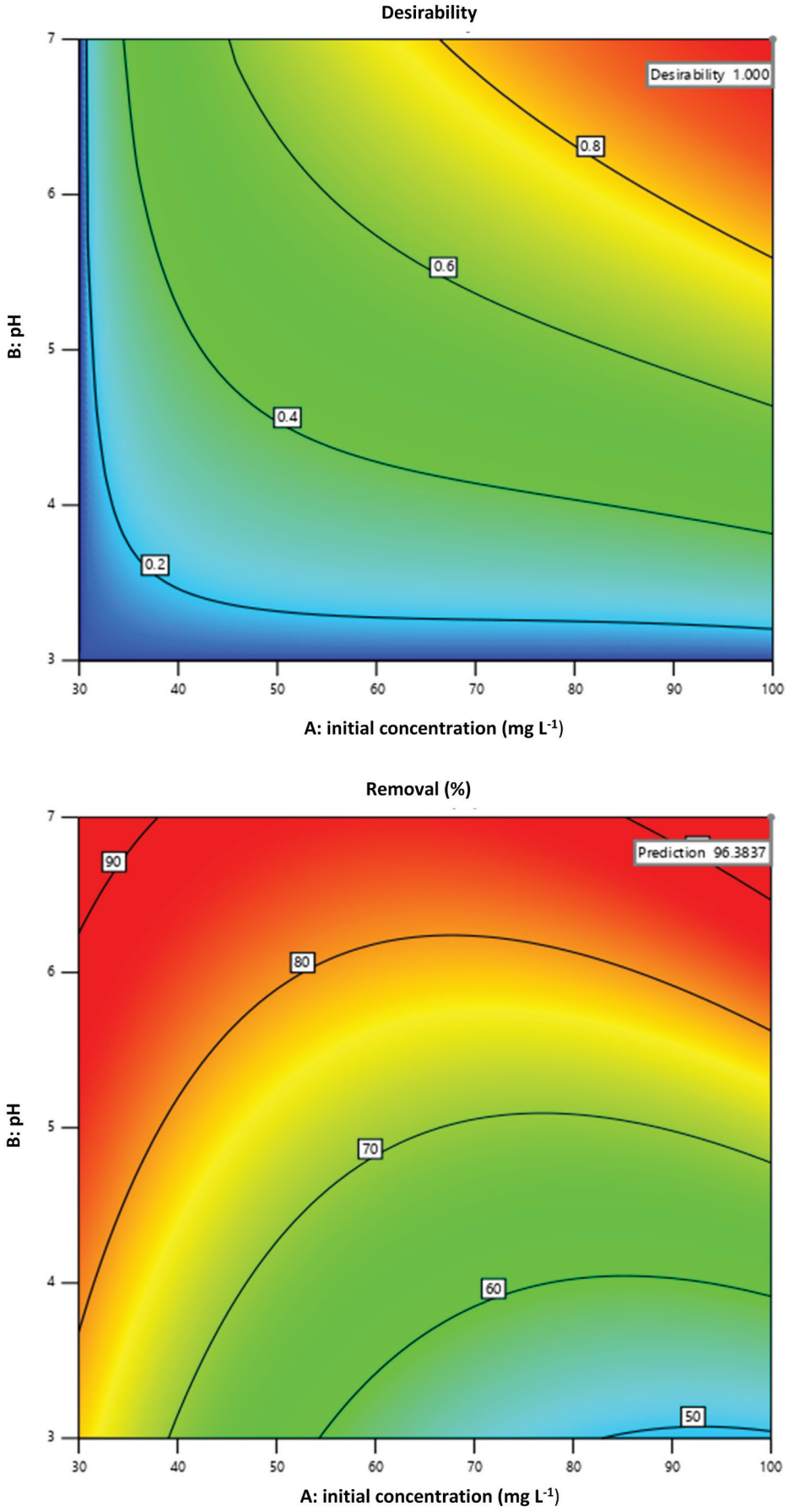

Fig. 10 – *2D contour plot corresponding to the predicted optimum removal % and the function desirability*

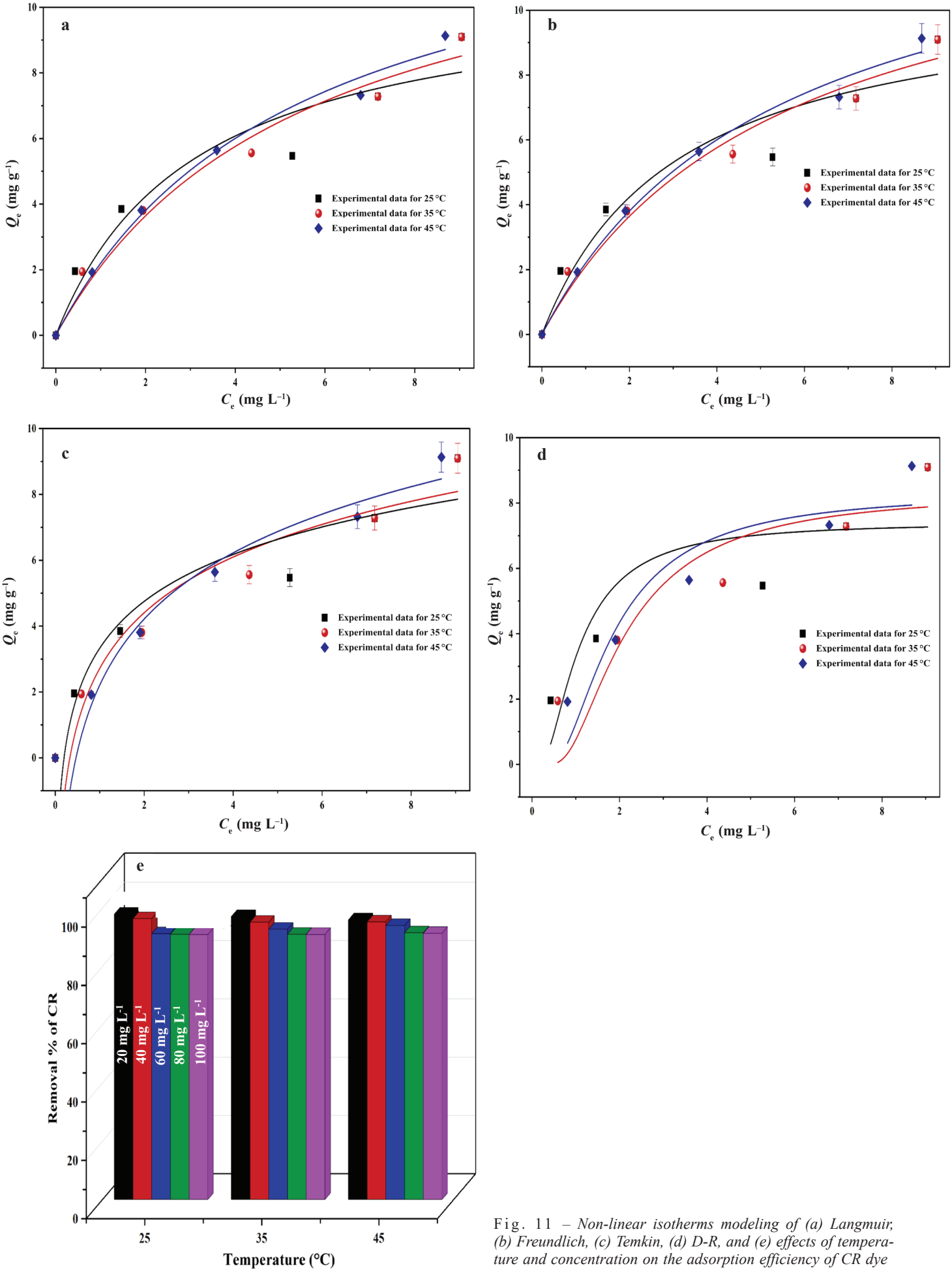

Fig. 11 – *Non-linear isotherms modeling of (a) Langmuir, (b) Freundlich, (c) Temkin, (d) D-R, and (e) effects of temperature and concentration on the adsorption efficiency of CR dye*

distribution of adsorption energies, indicating the presence of multiple active sites on the ZLS surface[56]. Furthermore, the K_F values suggest a moderate adsorption capacity of the surface, while the 1/n values <1 indicate favorable adsorption[59,60].

The Langmuir isotherm (Fig. 11a) shows good agreement with the experimental data, especially at higher temperature (R^2= 0.99134, χ^2 = 0.1255), suggesting that the adsorption process became more uniform, with monolayer formation occurring on a homogeneous surface[61]. This result can be attributed to the hypothesis that higher temperatures increase the mobility of molecules, facilitating their reach to the most favorable sites on the surface, resulting in a more ordered monolayer adsorption process[7,62]. The model also provided estimates of the maximum adsorption capacity Q_{max}, which were 10.76, 13.73, and 14.19 mg g^{-1} at 25, 35, and 45 °C, respectively. The Temkin isotherm model (Fig. 11c), applied to incorporate interactions between adsorbed molecules, assumed that the heat of adsorption decreases linearly with surface coverage[1]. The positive B_T values suggest that the adsorption process was exothermic[63,64], supporting the results obtained from the temperature study. The R^2 values of 0.89, 0.93, and 0.97 for the same temperatures, indicate an adequate agreement with the experimental data and improvement with increasing temperature. These findings do not contradict the exothermic nature of the process. Although the D-R model (Fig. 11d) was originally developed for microporous materials[65], its application to the ZLS adsorbent still provided valuable information regarding the adsorption mechanism. The low adsorption energy values (E < 8 kJ mol^{-1}) obtained at all investigated temperatures (25, 35, and 45 °C) and the good fit of Langmuir isotherm indicate that the adsorption process was mixed in nature involving both chemisorption and physisorption[63,64].

Kinetics study

Fig. 12a illustrates the adsorption capacity of CR dye onto the ZLS adsorbent at different contact times based on the experimental data. The experiments were conducted with a dye concentration of 100 mg L^{-1}, a solution dose of 1 g/0.1 L, a pH of 7, and contact times ranging from 0 to 180 minutes. The Q_t values increased rapidly within the first 60 min due to the abundance of active sites, then gradually approached equilibrium as the ZLS surface became saturated[11]. Kinetic analysis, based on the nonlinear data presented in Fig. 12a and Table 6, showed that both the pseudo-first-order (PFO) and pseudo-second-order (PSO) models described the experimental data well. The correlation coefficients were R^2 = 0.99547 for the PFO model and R^2 = 0.99669 for the PSO model, indicating that the PSO model provided a slightly better description of the adsorption process. Furthermore, the experimental equilibrium adsorption capacity (Q_e = 9.39 mg g^{-1}) closely matched the PSO predicted value (9.30101 mg g^{-1}) and the PFO predicted value (9.25601 mg g^{-1}). These findings suggest that, while physical adsorption dominated the initial stage[66], chemisorption involving electron sharing or exchange also contributed significantly to the overall rate-controlling mechanism[48]. These observations are consistent with the isotherm analysis results.

Fig. 12b and Table 6 present the intraparticle diffusion model (IPD) analysis. The IPD plot exhibited multilinear behavior with three distinct regions corresponding to external surface adsorption, gradual intraparticle diffusion, and final equilibrium. However, the correlation coefficients for these regions (R^2 = 0.86, R^2 = 0.99, and R^2 = 0.84, respectively) indicate that intraparticle diffusion alone failed to fully describe the adsorption process. In addition, the deviation of the plots from the origin (C≠0) confirmed that IPD was not the predominant rate-controlling step[48], and that boundary-layer effects also played an important role. Collectively, the adsorption process can be described as a mixed mechanism involving both physisorption and chemisorption.

Thermodynamic modeling

The thermodynamic investigation presented in Fig. 13 and Table 7 was conducted to validate the obtained results and establish coherence among the overall results Based on the optimization analysis and the pronounced effect of temperature on adsorption behavior, suitable experimental conditions were selected for the thermodynamic analysis. The negative enthalpy change ΔH^0 = –11.0959 kJ mol^{-1} suggested the exothermic nature of the process[63]. Furthermore, ΔH^0 < 40 mol^{-1} confirmed the physisorption process[67]. The negative Gibbs free energy values (ΔG^0) confirmed the spontaneous nature of the adsorption process[15]. The calculated ΔG^0 values of –2.27893, –1.9836, and –1.68719 mol^{-1} at 25, 35, and 45 °C, respectively, demonstrated that adsorption was thermodynamically feasible over the investigated temperature range. The decrease in the magnitude of ΔG^0 with increasing temperature indicates a reduction in the adsorption driving force. The negative entropy change (ΔS^0 = –29.6 J mol^{-1} K^{-1}) provided further insight into the process, reflecting a reduction in system randomness at the solid-solution interface, as CR dye molecules lose degrees of freedom and become more ordered upon immobilization on the ZLS surface[60,68]. Overall, the thermodynamic results demonstrated that the adsorption process was spontaneous, exothermic, and predominantly driven by physical interactions.

Table 5 – *Experimental isotherm parameters of CR dye adsorption onto ZLS adsorbent*

Isotherm	Parameter	Temperature		
		25 °C	35 °C	45 °C
Langmuir	Q_{L-M} (mg g^{-1})	10.76396 ± 2.2687	13.73118 ± 2.4463	14.18657 ± 1.51503
	K_L (L mg^{-1})	0.32404 ± 0.19408	0.18056 ± 0.06751	0.1834 ± 0.03983
	χ – Square	0.88069	0.30828	0.12556
	R^2	0.93805	0.97844	0.99134
Freundlich	K_F ((mg g^{-1})(L mg^{-1})$^{-1/n}$)	2.79853 ± 0.51668	2.4852 ± 0.22331	2.50293 ± 0.23374
	1/n	0.49935 ± 0.0958	0.57064 ± 0.04694	0.58939 ± 0.05019
	χ-Square	0.55229	0.11601	0.14228
	R^2	0.94716	0.989	0.98674
Temkin	B_T (J mol^{-1})	2.05522 ± 0.41243	2.44055 ± 0.38379	2.89828 ± 0.28004
	A_T (L g^{-1})	5.05022 ± 2.97432	3.04203 ± 1.18807	2.14143 ± 0.43666
	χ-Square	1.12664	0.72831	0.29231
	R^2	0.89221	0.93094	0.97275
Dubinin–Radushkevich	Q_{D-M} (mg g^{-1})	7.39679 ± 1.03337	8.32383 ± 1.18045	8.31689 ± 0.90635
	K_{D-R} (mol^2 kJ^{-2})	1.68152 ± 1.16479	4.98538 ± 2.74159	3.95268 ± 1.55857
	E (kJ mol^{-1})	0.5453	0.3167	0.3557
	χ-Square	2.74464	2.19339	1.37547
	R^2	0.73741	0.79201	0.8718

Table 6 – *Experimental kinetic parameters of CR dye adsorption onto ZLS adsorbent*

Kinetic model		Parameter	
PFO		Q_e (mg g^{-1}) K_1 (min^{-1}) R^2	9.25601±0.04633 3.25689±0.48505 0.99547
PSO		Q_e (mg g^{-1}) K_2 (min g mg^{-1}) R^2	9.30101±0.04193 1.8527±0.55236 0.99693
IPD	Stage 1 Boundary layer diffusion	K_{ID1} C_1 R^2	0.10963±0.0432 8.80357±0.07495 0.8652
	Stage 2 Intraparticle diffusion	K_{ID2} C_2 R^2	0.09238±0.00284 8.74187±0.01269 0.99718
	Stage 3 Equilibrium	K_{ID3} C_3 R^2	0.01091±0.00271 9.31782±0.02852 0.84397

Table 7 – *Experimental thermodynamic parameters of CR dye adsorption onto ZLS adsorbent*

Adsorbent	ΔH^0 (kJ mol^{-1})	ΔS^0 (J mol^{-1} K^{-1})	ΔG^0(kJ mol^{-1})		
			298 K	308 K	318 K
ZLS	–11.0959	–29.587	–2.27893	–1.9836	–1.68719

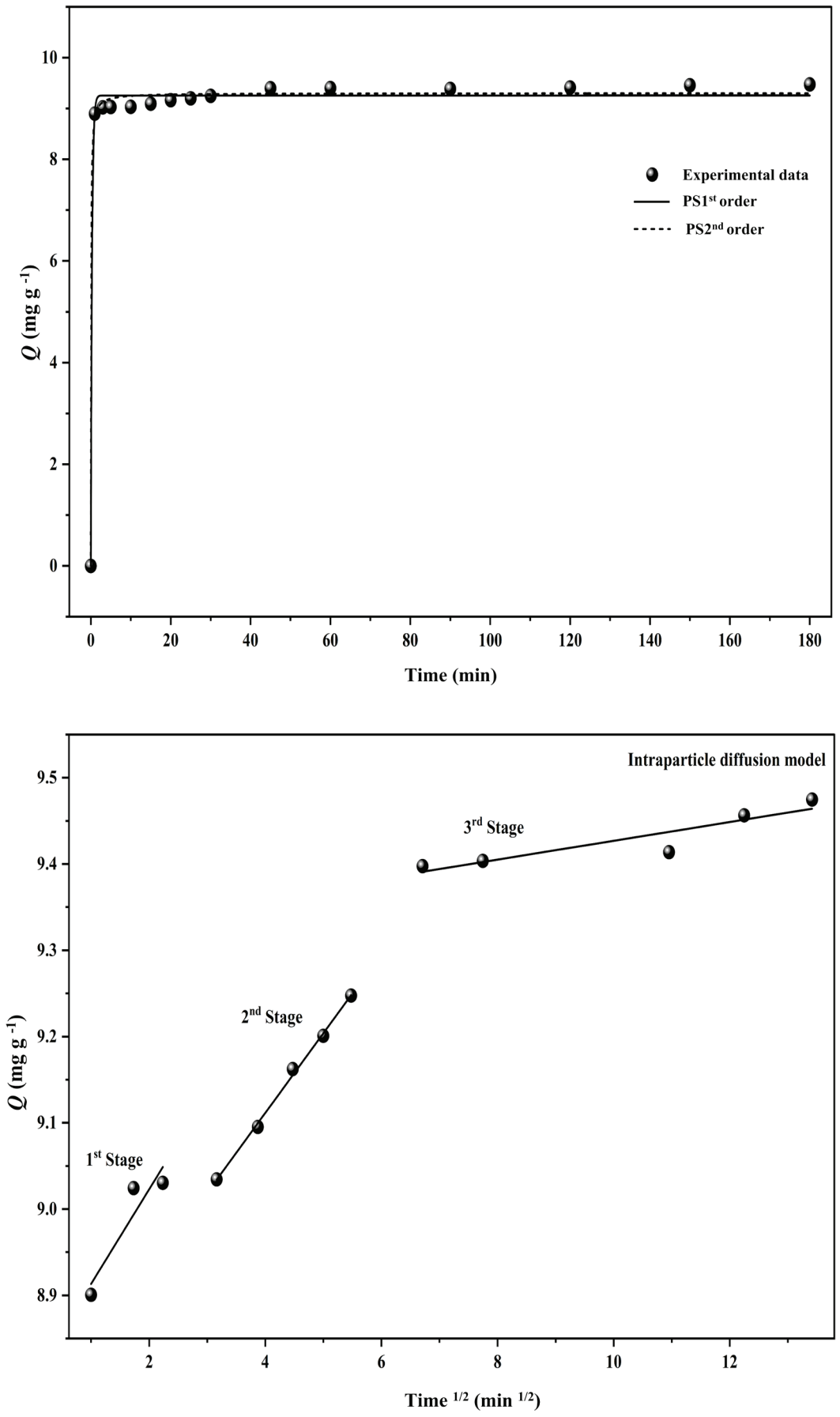

Fig. 12 – *Representations of the PFO, PSO, and IPD kinetic models*

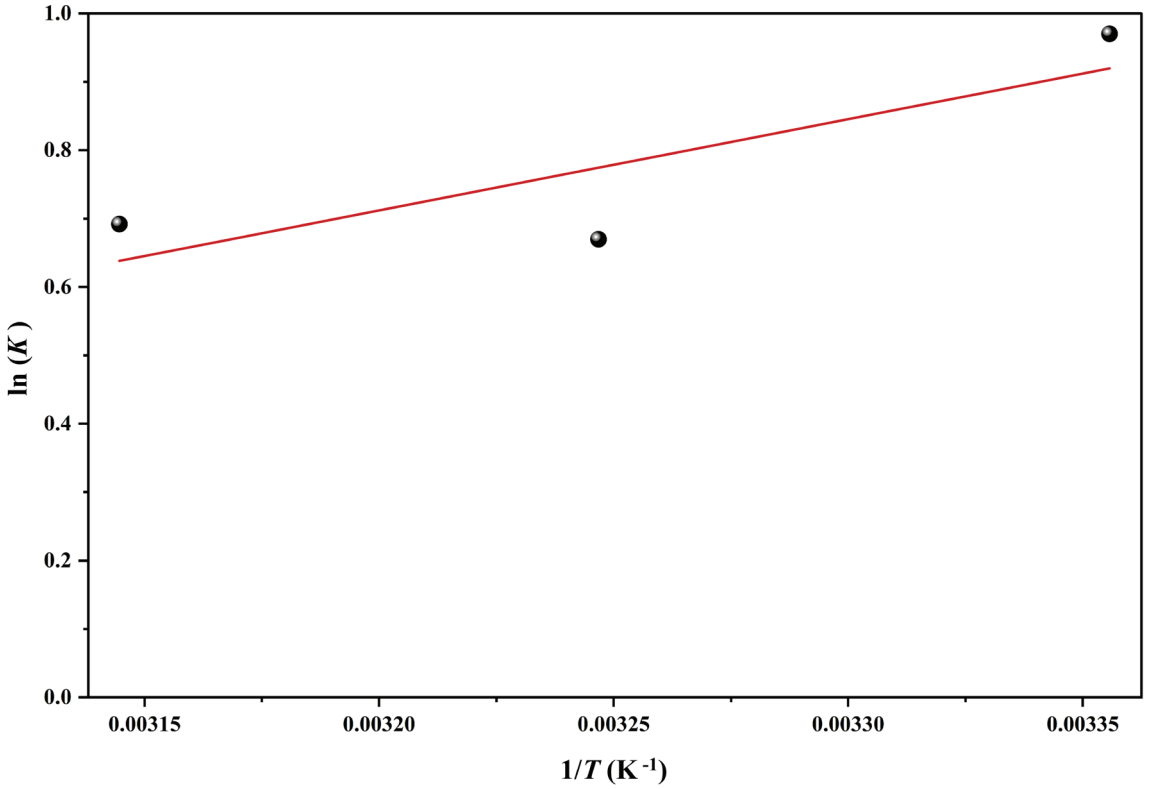

Fig. 13 – *Van't Hoff plot of 1/T vs ln(K) for the adsorption of CR dye onto the ZLS adsorbent*

Elucidation of the adsorption mechanism

Understanding the adsorption mechanism of CR dye onto the ZLS adsorbent is crucial for elucidating the interfacial interactions and molecular-scale processes governing adsorption efficiency (Fig. 14). The adsorption process was predominantly influenced by the adsorbent characteristics, including the functional groups, structural morphology, and the pH of the CR dye solution, as well as by the diffusion behavior of dye molecules toward available active sites or textural features[69]. BET analysis demonstrated that ZLS possessed a mesoporous structure with an average pore size of 4.35 nm and a high specific surface area, both of which facilitated the diffusion of CR molecules and increased the accessibility of adsorption sites. Most importantly,

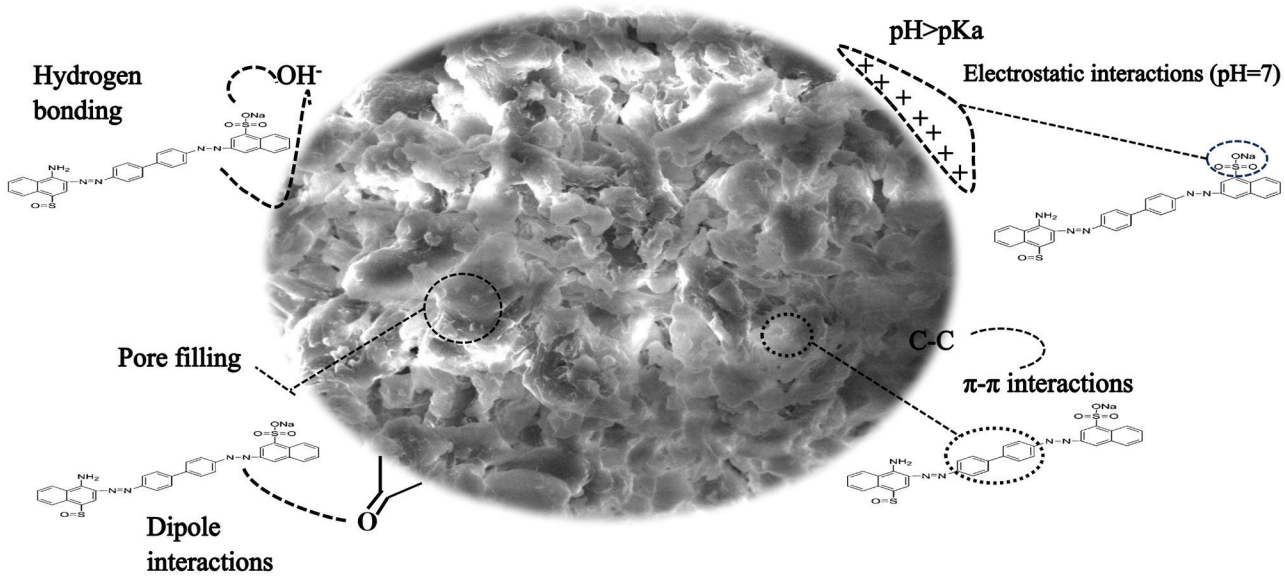

Fig. 14 – *Schematic representation of the proposed adsorption mechanism of CR dye on the ZLS surface*

the FTIR analysis before and after adsorption confirmed the presence of hydrogen bonding mainly originating from C=C, C=O and hydroxyl (–OH) groups abundant in cellulose and hemicellulose. This was evidenced by the shift in the OH stretching band from 3395 to 3433 cm^{-1} accompanied by an increase in intensity increase[7,42]. Adsorbed complexes may also form due to the carboxyl (–COOH) groups present in lignin and the amino groups derived from the plant or amino-containing biopolymers; these functional groups can interact with oxygen and nitrogen atoms in CR molecules. In addition, the presence of nonpolar aromatic domains within the lignin structure facilitated hydrophobic and π-π interactions with the aromatic CR dye molecules, contributing significantly to overall adsorption affinity[70]. The good fit of the Freundlich isotherm model indicated the heterogeneous nature of the ZLS adsorbent surface, as also confirmed by SEM analysis, and suggested the possibility of multilayer adsorption, which is typically described as physisorption, validating the Van der Waals, dipole-dipole, and π-π interactions between the adsorbent surface and the adsorbate[61]. On the other hand, the strong fit of the Langmuir isotherm model with a coefficient of regression superior to 0.9, indicated the contribution of chemisorption within a monolayer adsorption to the overall adsorption process. Solution pH represents a key factor to describe the adsorption mechanism because it directly affects both the surface of the ZLS adsorbent and the protonation-deprotonation behavior of the CR dye[15]. In this study, multiple interrelated parameters were found to influence the determination of the optimum pH value of the adsorption process, including the pH_{pzc} of the ZLS adsorbent, the pKa of CR dye solution, color transition region of CR dye solution, the avoidance of highly acidic and basic regions that could introduce competition between negatively charged CR dye molecules and H^+ or OH^- of NaOH or HCl respectively, the adsorption efficiency, process cost, and environmental considerations. At neutral pH 7, the reaction medium is in equilibrium with the H^+, enhancing the electrostatic attractions, but the reaction is mainly governed by π-π interactions, weak hydrogen bonding, Van der Waals interactions, and the ionized SO_3^- of the CR dye molecules[7].

Comparative study of Congo Red removal (Q_{max}) using ZLS and other adsorbents

The data summarized in Table 8 compare the key experimental conditions for CR dye removal and the maximum adsorption capacities (Q_{max}) derived from relevant literature using various adsorbents. *Ziziphus lotus* stone (ZLS), as a raw plant-based adsorbent used in its natural form, exhibited adsorption capacities exceeding 10–14 mg g^{-1}, demonstrating competitive performance relative to chemically modified adsorbents, synthetic activated carbons, and advanced nanomaterials[5,74]. ZLS also exhibited higher adsorption capacities than several other natural adsorbents[22,24,26,71,72,75]. Although some

Table 8 – *Comparison of the maximum adsorption capacity of the ZLS adsorbent for CR dye removal with other adsorbents reported in the literature*

Adsorbent	Experimental conditions	Q_{max} (mg g^{-1})	Isotherm model	Reference
Roots of *Eichhornia crassipes*	1 g, 50 mL, 200 rpm, 104.502 mg L^{-1}, and 90 min	1.58	Freundlich	[65]
Tunics of the corm of saffron	0.5 g, 50 mL, pH = 10, 100 mg L^{-1}, and 60 min	6.2	Langmuir	[20]
Rice husk	0.75 g, 25 mL, pH = 3–5, 100 mg L^{-1}, and 60 min	0.883	Temkin	[66]
Calcined kaolin clay	0.75 g, 25 mL, pH = 3–5, 100 mg L^{-1}, and 60 min	2.194	Temkin	[66]
Microwaved rice husk-clay hybrid	0.75 g, 25 mL, pH = 3–5, 100 mg L^{-1}, and 60 min	4.008	Temkin	[66]
Metal oxide/clay nanocomposites	1 g, 100 mL, 120 mg L^{-1}, 250 rpm, and 10 min	11.2	Langmuir	[5]
Fly ash	1 g, 1 L, 200 rpm, 10 mg L^{-1}, and 60 min	22.12	Langmuir	[67]
Tetraethylenepentamine-modified peanut husks composite beads	0.2 g, 20 mL, 150 rpm, 100 mg L^{-1}, and 60 min	19.57	Freundlich	[53]
HNO_3-modified resorcinol – formaldehyde carbon gels	0.03 g, 20 mL, and 5 days	10.58	Langmuir	[68]
Pine bark	10 g, 1 L, 100 rpm, pH = 6, 5 mg L^{-1}, and 7 days	3.92	Freundlich	[24]
NaOH-activated natural glauconite	0.02 g, 20 mL, 5–25 mg L^{-1}, pH = 7, and 360 min	5.1–13.2	Freundlich	[69]
Banana peel	1.5 g, 80 mL, 200 rpm, pH = 10, 20 mg L^{-1}, and 90 min	1.721	Langmuir	[22]
Ziziphus lotus stone	0.5 g, 50 mL, 150 rpm, pH = 7, and 60 min	10.76 – 14.19	Freundlich	This study

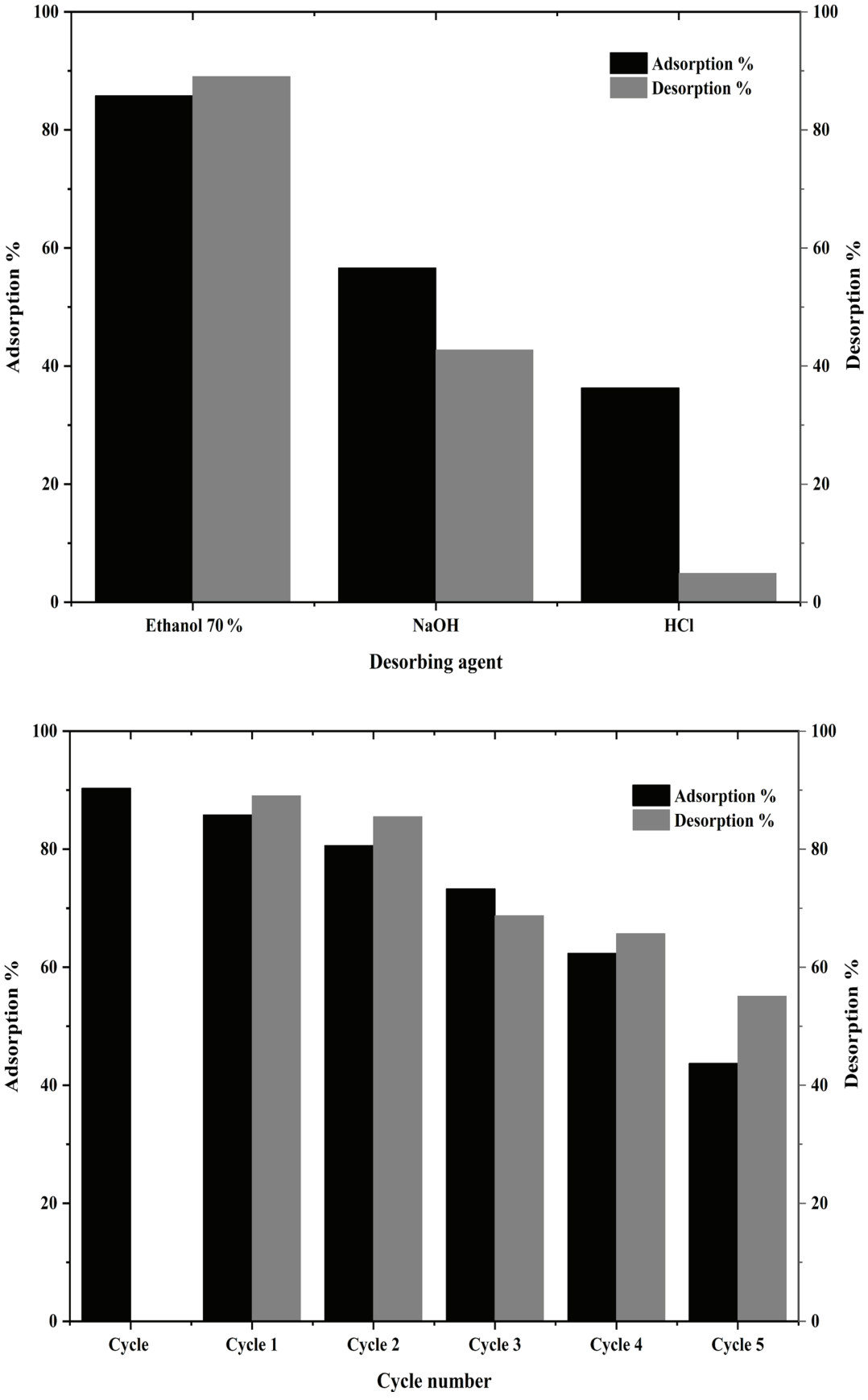

Fig. 15 – *Desorption and reusability diagrams*

highly engineered materials and combustion-derived byproducts have achieved superior adsorption capacities[58,73] these materials generally require costly and energy-intensive preparation processes. Therefore, the ZLS adsorbent investigated in this study provides an optimal balance between adsorption efficiency, environmental compatibility, and economic feasibility, making it a promising candidate for large-scale wastewater treatment applications.

Desorption and reusability studies

Evaluating desorption efficiency and adsorbent reusability is essential for assessing its long-term operational stability and suitability in cyclic adsorption applications. In this study, 70 % ethanol, as shown in Fig. 15, demonstrated superior regeneration performance, achieving desorption efficiencies of approximately 87 % while maintaining an adsorption capacities close to 85 %, highlighting the ability of moderately polar organic solvents to effectively disrupt adsorbate-adsorbent interactions without compromising the structural integrity of the adsorbent[66]. The adsorption efficiency and desorption efficiency were calculated using the following equations[33]:

$$\text{Adsorption efficiency}(\%) = \frac{C_0 - C_e}{C_0} \cdot 100 \quad (22)$$

$$\text{Desorption}(\%) = \frac{C_D}{C_0 - C_e} \quad (23)$$

where: C_0 is the initial adsorbate concentration, C_e is the equilibrium concentration after adsorption, and C_D is the amount of CR dye molecules desorbed from the ZLS adsorbent. In contrast, strong alkaline (NaOH) and acidic (HCl) eluents significantly reduced both adsorption and desorption efficiencies, effects that can be attributed to chemical modifications of active ZLS surface sites. Specifically, acidic and basic conditions can disrupt the surface functional groups. The reusability of the adsorbent was evaluated over five consecutive regeneration cycles (Fig. 1). However, both adsorption and desorption efficiencies gradually decreased after each subsequent cycle, reaching approximately 45 % by fifth cycle.

Cost estimation study

Ziziphus lotus stone (ZLS) demonstrated high efficiency as a biosorbent for Congo Red (CR) dye removal from aqueous medium, achieving 95 % removal efficiency. The reuse of the ZLS agricultural byproducts as adsorbents instead of their uncontrolled disposal provides significant environmental benefits by reducing agricultural waste generation and promoting sustainability. Therefore, a cost analysis was conducted to evaluate the feasibility and practical applicability of the developed adsorption system as a competitive and environmentally friendly alternative to activated carbon[76,77].

Table 9 – *ZLS adsorbent cost per kg (Esmati et al.)*[71]

Partial element	Electricity cost ($/kWh)	Energy consumption (kWh)	Unit cost per kg ($/kg)
Grinding	0.036	0.44 kW/0.35 h	0.01584
Drying	0.036	2.7 kW/24 h	0.0972
Chemicals	–	–	0
Net cost	–	–	0.11304
Total cost	–	–	0.11304

ZLS adsorbent cost estimation

The production cost of the ZLS adsorbent was primarily associated with the energy requirements for grinding and drying (105 °C, 24 h). No additional chemical or physical treatments of the ZLS adsorbent were applied during adsorbent preparation, and the raw material itself was considered cost-free at the source because it originated from agricultural waste. Table 9 summarizes the estimated production costs of the ZLS adsorbent based on the Algerian industrial electricity tariff of 0.036 USD/kWh in 2024.

The results presented in Table 8 indicate that the production cost of 1 kg of ZLS adsorbent was 0.11304 USD/kg. These results highlight the strong economic potential of the ZLS adsorbent, particularly when compared with chemically treated activated carbon reported in a recent study by Mihret *et al.* (8 USD/kg)[72], or the commercial activated carbon that typically costs 12 USD/kg [78,79], making it approximately 70 to 100 times more expensive than the ZLS adsorbent. This substantial difference underscores ZLS adsorbent value as a highly cost-effective product.

Adsorption process estimation cost

The total cost of the adsorption process was estimated as the sum of the amortization cost of the investment (ACin) and the operating cost (OC) [80,81]. The annual amortization cost (AAC), amortization cost (AC), and the capital recovery factor (CF) were calculated using the following equations[80,81]:

$$\text{AAC} = \text{AC} \cdot \text{CF} \quad (24)$$

$$\text{AC} = \frac{C_r \cdot V_r}{n \cdot V_t} \quad (25)$$

$$\text{CF} = \frac{i \cdot (1+i)^n}{(1+i)^n - 1} \quad (26)$$

where:

C_r is the cost per cubic meter of the processing unit, estimated to be 2,500 USD/m^3

n is the estimated lifespan of the adsorption unit (15 years)

V_t is the annual wastewater treatment volume, estimated at approximately 600 m^3/year (2 m^3/day)

V_r is the adsorption reactor capacity m^3, calculated using Equation 27

i is the annual interest rate (5 %) kW

$$V_r = \frac{V_t \cdot t_{exp}}{D \cdot t_w} \quad (27)$$

where:

t_{exp} is the duration of one batch adsorption cycle, determined previously in this study (1 h), D is the total number of service days (300 days/year), and t_w is service hours per day (12 h/day).

The amortization cost includes construction expenses as well as electrical and mechanical installation costs[80]. Based on the adopted data, the AC value was estimated at 0.046 USD/m^3 while the annual amortization cost for wastewater treatment was 0.0045 USD/m^3. The operating cost (OC) included used chemicals, labor expenses, energy consumption, and adsorbent life duration. In this study, no chemicals were used, and labor expenses were excluded from the analysis, as the adsorption process does not involve significant labor requirements. Thus, the OC was estimated mainly from energy consumption (\$/m^3) and the maintenance expenses.

Therefore, the adsorbent regeneration cost was included in the energy demand only for ZLS adsorbent, which was approximately 2 % of the amortization cost. The operating cost was calculated using Equation 28:

$$O_C = E_C + \frac{2\ AC}{100} \quad (28)$$

The energy consumption cost E_C (USD/m^3) associated with pumps, mixers, and adsorbent regeneration drying was calculated using Equation 29:

$$E_C = \frac{P_E \cdot E \cdot D \cdot t_w}{V_t} \quad (29)$$

where: P_E is the electricity unit price in Algeria (0.036 USD/kWh in 2024), E is the energy consumption (kW). The resulting E_C value was 0.0648 USD/m^3 corresponding to 59 % of the total adsorption process cost. Consequently, the total cost of the designed adsorption process was estimated at 0.112 USD/m^3. These findings demonstrate the strong potential of the ZLS adsorbent as an environmentally friendly and cost-effective material for large-scale industrial applications.

Conclusions

The present study demonstrates the high performance and low production cost of the *Ziziphus lotus* stone (ZLS) adsorbent, which exhibited excellent structural stability, abundant surface functional groups, and remarkable adsorption efficiency for Congo Red (CR) dye removal. Optimization using the Box-Behnken Design (BBD) improved the adsorption performance by 10 %, achieving over 95 % removal efficiency under the optimal conditions of 100 mg L^{-1} initial dye concentration, 0.5 g adsorbent dosage, and solution pH 7. Nonlinear isotherm analysis revealed that both the Freundlich and Langmuir models adequately described the adsorption behavior, suggesting multilayer adsorption on the ZLS adsorbent surface together with chemisorption and physisorption mechanisms. The maximum adsorption capacity was around 11 mg g^{-1} at 25 °C. The chemical behavior was confirmed by the kinetic PSO model. Furthermore, thermodynamic analyses showed that the adsorption process was spontaneous, favorable, exothermic, and associated with decreased randomness at the adsorbent-adsorbate interface.

To further valorize the ZLS adsorbent, the cost analysis revealed a low production cost of 0.11304 USD/kg, nearly one hundred times lower than the market price of commercial activated carbon. The total adsorption process costs were estimated at 0.112 USD/m^3 for a projected system lifespan of 15 years. These findings indicate that the agricultural byproduct ZLS, used as an adsorbent, is a promising, eco-friendly, economically viable, and locally abundant material, which reinforces its economic and environmental attractiveness for large-scale and sustainable applications.

References

1. *Das, K., Sukul, U., Chen, J. S., Sharma, R. K., Banerjee, P., Dey, G., Taharia, Md., Wijaya, C. J., Lee, C.-I., Wang, S. L., Nuong, N. H. K., Chen, C. Y.*, Transformative and sustainable insights of agricultural waste-based adsorbents for water de-fluoridation: Biosorption dynamics, economic viability, and spent adsorbent management, Heliyon. **10** (2024) e29747. doi: https://doi.org/10.1016/j.heliyon.2024.e29747
2. *Boudaoud, A., Ad, C., Djedid, M., Guermit, M., Benalia, M., Soltani, A.,* Efficient removal of cationic micro-pollutant using sodium-linked mesoporous adsorbent: Characterisation, kinetic and isotherm studies, Russ. J. Phys. Chem. A. **99** (2025) 727. doi: https://doi.org/10.1134/S0036024424604403
3. *Lin, L., Yang, H., Xu, X.,* Effects of water pollution on human health and disease heterogeneity: A review, Front. Environ. Sci. **10** (2022) 880246. doi: https://doi.org/10.3389/fenvs.2022.880246
4. *Nazish, M. A., Khan, M. K., Mazhar, B., Mustafa, M.,* Impact of water pollution on waterborne infections: Emphasizing microbial contamination and associated health hazards in humans, Discov. Water. **5** (2025) 19. doi: https://doi.org/10.1007/s43832-025-00198-x

5. *Rasilingwani, T. E., Gumbo, J. R., Masindi, V., Foteinis, S.*, Removal of Congo red dye from industrial effluents using metal oxide-clay nanocomposites: Insight into adsorption and precipitation mechanisms, Water. Resour. Ind. **31** (2024) 100253. doi: https://doi.org/10.1016/j.wri.2024.100253
6. *Kumar, M., Mishra, A., Patel, S. K., Mishra, V., Kushwaha, J., Singh, S., Singh, D., Singh, V., Giri, B. S., Singhania, R. R., Singh, D.,* Environmental impacts and strategies for bioremediation of dye-containing wastewater, Bioeng. **12** (2025) 1043. doi: https://doi.org/10.3390/bioengineering12101043
7. *Sudarsan, S., Murugesan, G., Varadavenkatesan, T., Vinayagam, R., Selvaraj, R.,* Efficient adsorptive removal of Congo Red dye using activated carbon derived from *Spathodea campanulata* flowers, Sci. Rep. **15** (2025) 1831. doi: https://doi.org/10.1038/s41598-025-86032-9
8. *Grouli, A., Chraka, A., Bachra, Y., Elkouali, M., Chtita, S., Berrada, M.,* An investigation of the adsorption of Congo red dye on two naturally occurring adsorbents hydroxyapatite and bentonite: An experimental analysis, DFT calculations, and Monte Carlo simulation, Heliyon. **10** (2024) e39884. doi: https://doi.org/10.1016/j.heliyon.2024.e39884
9. *Ozturk, E.,* Improving water-use efficiency and environmental performances in an integrated woven-knitted fabric printing-dyeing textile mill, J. Clean. Prod. **379** (2022) 134805. doi: https://doi.org/10.1016/j.jclepro.2022.134805
10. *Siddiqui, S., Allehyani, E. S., Al-Harbi, S. A., Rajor, H. K., Oh, S., Hasan, Z., Abomuti, M.,* Investigation of Congo Red toxicity towards different living organisms: A review, Proc. **11** (2023) 807. doi: https://doi.org/10.3390/pr11030807
11. *Madan, S., Shaw, R., Tiwari, S., Tiwari, S. K.,* Adsorption dynamics of Congo red dye removal using ZnO functionalized high silica zeolitic particles, Appl. Surf. Sci. **487** (2019) 907. doi: https://doi.org/10.1016/j.apsusc.2019.04.273
12. *Liu, Y. Y., Li, Z., Liang, Y., Zhuang, J. H., Zhang, W. J., Tang, T., Cheng, Y. F., Ou, R., Zhang, B. Y., Ou, J. Z.,* Synergistic engineering of four-pointed star-like layered stacking and oxygen vacancies toward high-efficiency Bi_2O_2-xSe photocatalysts for the degradation of tetracycline and congo red, J. Environ. Chem. Eng. **13** (2025) 117866. doi: https://doi.org/10.1016/j.jece.2025.117866
13. *Chequer, F. M. D., Lizier, T. M., de Felico, R., Zanoni, M. V. B., Debonsi, H. M., Lopes, N. P., Marcos, R., de Oliveira, M. D. P.,* Analyses of the genotoxic and mutagenic potential of the products formed after the biotransformation of the azo dye Disperse Red 1, Toxicol. In Vitro. **25** (2011) 2054. doi: https://doi.org/10.1016/j.tiv.2011.05.033
14. *Sarkar, S., Banerjee, A., Halder, U., Biswas, R., Bandopadhyay, R.,* Degradation of synthetic azo dyes of textile industry: A sustainable approach using microbial enzymes, Water Conserv. Sci. Eng. **2** (2017) 121. doi: https://doi.org/10.1007/s41101-017-0031-5
15. *Hammad, W. A., Darweesh, M. A., Zouli, N., Osman, S. M., Eweida, B., Amr, M. H. A.,* Adsorption of cationic dye onto Raphanus seeds: Optimization, adsorption kinetics, thermodynamic studies, Sci. Rep. **14** (2024) 17827. doi: https://doi.org/10.1038/s41598-024-66761-z
16. *Sayadi, S., Brouillette, F.,* Multifunctional cellulose fibers for the simultaneous removal of metal cations and anions: Adsorption study, J. Environ. Chem. Eng. **13** (2025) 119608. doi: https://doi.org/10.1016/j.jece.2025.119608
17. *Chou, M. Y., Lee, T. A., Lin, Y. S., Hsu, S. Y., Wang, M. F., Po, H., Li, P., Huang, H., Lu, W. C., Ho, J. H.,* On the removal efficiency of copper ions in wastewater using calcined waste eggshells as natural adsorbents, Sci. Rep. **13** (2023) 437. doi: https://doi.org/10.1038/s41598-023-27682-5
18. *Gargiulo, V., Di Natale, F., Alfe, M.,* From agricultural wastes to advanced materials for environmental applications: Rice husk-derived adsorbents for heavy metals removal from wastewater, J. Environ. Chem. Eng. **12** (2024) 113497. doi: https://doi.org/10.1016/j.jece.2024.113497
19. *Kelly, W. K. S., Alvin, L. T. Z., Karen, B. J., Tan, T. H., Eric, L. T. C., Jacqueline, L., Yoshito, A.,* Duckweed-derived magnetic adsorbent for efficient removal of methylene blue, Biomass Conv. Bioref. **16** (2026) 111. doi: https://doi.org/10.1007/s13399-025-06946-2
20. *Karen, B. J., Alvin, L. T. Z., Tan, T. H., Kelly, W. K. S., Eric, L. T. C., Alvin, L. T. Z., Karen, B. J., Tan, T. H., Jacqueline, L., Yoshito, A.,* Sustainable dye wastewater treatment: Utilizing duckweed-derived adsorbents for efficient methylene blue removal, Biomass Conv. Bioref. **15** (2025) 19157. doi: https://doi.org/10.1007/s13399-024-06432-1
21. *Etim, U. J., Umoren, S. A., Eduok, U. M.,* Coconut coir dust as low-cost adsorbent for the removal of cationic dye from aqueous solution, J. Saudi Chem. Soc. **20** (2016) S67. doi: https://doi.org/10.1016/j.jscs.2012.09.014
22. *Dbik, A., Bentahar, S., El Khomri, M., El Messaoudi, N., Lacherai, A.,* Adsorption of Congo red dye from aqueous solutions using tunics of the corm of the saffron, Materials Today: Proc. **22** (2020) 134. doi: https://doi.org/10.1016/j.matpr.2019.08.148
23. *Baby, R., Saifullah, B., Hussein, M. Z.,* Palm Kernel Shell as an effective adsorbent for the treatment of heavy metal contaminated water, Sci. Rep. **9** (2019)18955. doi: https://doi.org/10.1038/s41598-019-55099-6
24. *Namasivayam, C., Kanchana, N.,* Removal of Congo red from aqueous solution by waste banana pith, Pertanika. J. Sci & Technol. **1** (1993) 33.
25. *Zareei, J., Juraev, N., Widatalla, S. T. H., Kerwad, M., Bokov, D. O., Alkhuzai, K. A., Benites, C. R., Alhadrawi, M., Al-Abdeen, S. H. Z.,* Investigation of the potential of pomegranate peel as a treatment option for heavy metal contaminated wastewater: Experimental and modeling approaches, Heliyon. **1** (2024) e34619. doi: https://doi.org/10.1016/j.heliyon.2024.e34619
26. *Litefti, K., Freire, M. S., Stitou, M., González-Álvarez, J.,* Adsorption of an anionic dye (Congo red) from aqueous solutions by pine bark, Sci. Rep. **9** (2019) 16530. doi: https://doi.org/10.1038/s41598-019-53046-z
27. *Ouldchikh, S., TirTouil, A., Meddah, B., Zizyphus lotus* (L.) Extracts as prebiotics in the aggregation and adhesion of probiotic and inhibition of pathogenic bacteria from patients with colorectal cancer, Int. J. Food Stud. **9** (1) (2020) 160. doi: https://doi.org/10.7455/ijfs/9.1.2020.a3
28. *Al Bsoul, A., Hailat, M., Abdelhay, A., Tawalbeh, M.,* Efficient removal of phenol compounds from the water environment using Ziziphus leaves adsorbent, Sci. Total Environ. **761** (2021) 143229. doi: https://doi.org/10.1016/j.scitotenv.2020.143229
29. *Boudechiche, N., Fares, M., Ouyahia, S., Yazid, H., Trari, M., Sadaoui, Z.,* Comparative study on removal of two basic dyes in aqueous medium by adsorption using activated carbon from *Ziziphus lotus* stones, Microchem J. **146** (2019) 1010. doi: https://doi.org/10.1016/j.microc.2019.02.010

30. *Yousif, S. A., Al-Mosawi, S.,* Adsorptive separation of dissolved cadmium from aqueous solution using (Ziziphus Spina-Christi) leaves as an adsorbent, S. Afr. J. Chem. Eng. **42** (2022) 12.
doi: https://doi.org/10.1016/j.sajce.2022.07.002
31. *Regti, A., Laamari, M. R., Stiriba, S., El Haddad, M.,* The potential use of activated carbon prepared from Ziziphus species for removing dyes from waste waters, Appl. Water. Sci. **7** (2017) 4099.
doi: https://doi.org/10.1007/s13201-017-0567-8
32. *Ferreira, S. L. C., Bruns, R. E., Ferreira, H. S., Matos, G. D., David, J. M., Brandaoa, G. C., da Silva, E. G. P., Portugal, L. A., dos Reis, P. S., Souza, A. S., dos Santos, W. N. L.,* Box-Behnken design: An alternative for the optimization of analytical methods, Anal. Chim Acta. **597** (2007) 179.
doi: https://doi.org/10.1016/j.aca.2007.07.011
33. *Nouacer, I., Hammadi, S., Benalia, M., Djedid, M., Bencheikh, S.,* Biosorption of carcinogenic metal ions using the immobilized microalgae *Auxenochlorella protothecoides* on a lignocellulosic matrix: Optimization, kinetic, isotherm and mechanism, S. Afr. J. Bot. **157** (2023) 297.
doi: https://doi.org/10.1016/j.sajb.2023.02.023
34. *Zahi, S., Ouazene, N., Tchekiken, C., Elaglia, W. F., Kerchich, Y., Belhaneche-Bensemra, N.,* Optimization of azithromycin degradation by Fenton oxidation: A comparative study of general full factorial design 3^3 and Box-Behnken design, React. Kinet. Mech. Catal. **136** (2023) 2147.
doi: https://doi.org/10.1007/s11144-023-02444-6
35. *Dada, A. O., Adekola, F. A., Odebunmi, E. O., Ogunlaja, A. S., Bello, O. S.,* Two–three parameters isotherm modeling, kinetics with statistical validity, desorption and thermodynamic studies of adsorption of Cu(II) ions onto zerovalent iron nanoparticles, Sci. Rep. **11** (2021) 16454.
doi: https://doi.org/10.1038/s41598-021-95090-8
36. *Lagergren, S.,* On the theory of so-called adsorption of dissolved substances, Kungl. Svenska Vetenskapsakad. Handl. **24** (1898) 1.
37. *Ho, Y. S., McKay, G.,* Pseudo-second-order model for sorption processes, process Biochen. **34** (1999) 451.
38. *Weber, W. J., Morris, J. C.,* kinetics of adsorption on carbon from solution, J. Sanitary Eng. Div. **89** (1963) 31.
39. *Abdelrazek, E. J. E., Gahlan, A. A., Gouda, G. A., Ahmed, A. S. A.,* Cost-effective adsorption of cationic dyes using ZnO nanorods supported by orange peel-derived carbon, Sci. Rep. **15** (2025) 4123.
doi: https://doi.org/10.1038/s41598-025-86209-2
40. *Boudaoud, A., Djedid, M., Benalia, M., Ad, C., Bouzar, N., Elmsellem, H.,* Removal of Nickel(II) and Cadmium(II) ions from wastewater by palm fibers, Chemi. Chemical. Eng. Biotechnol, Food Ind. **18** (2017) 391.
41. *Lee, S. M., Lee, S. H., Roh, J. S.,* Analysis of activation process of carbon black based on structural parameters obtained by XRD analysis, Crystals. **11** (2021) 153.
doi: https://doi.org/10.3390/cryst11020153
42. *Alzahrani, E. A., Nabi, A., Kamli, M. R., Albukhari, S. M., Althabaiti, S. A., Al-Harbi, S. A., Khan, I., Malik, M. A.,* Facile green synthesis of ZnO NPs and plasmonic Ag-supported ZnO nanocomposite for photocatalytic degradation of methylene blue, Water. **15** (2023) 384.
doi: https://doi.org/10.3390/w15030384
43. *Nouri, M., Griballah, I., Tahlaiti, M., Grondin, F., Beaugrand, J.,* Plant extraction and physicochemical characterizations of untreated and pretreated diss fibers (*Ampelodesmos mauritanicus*), J. Nat. Fibers. **18** (2019) 1083.
doi: https://doi.org/10.1080/15440478.2019.1687062
44. *Aderibigbe, D. O., Dabo, O. S., Akinwumi, V. O., Giwa, A. A.,* Competitive adsorption of Congo red by sawdust in the presence of reactive black 5 and the effect of ionic strength, Wat. Pract. Technol. **20** (2025) 1042.
45. *Zhang, J., Mariska, S., Pap, S., Tran, H. N., Chao, H.,* Enhanced separation capacity of carbonaceous materials (hydrochar, biochar, and activated carbon) toward potential toxic metals through grafting copolymerization, Sep. Purif. Technol. **320** (2023) 124229.
doi: https://doi.org/10.1016/j.seppur.2023.124229
46. *Kharchi, N., Barka, B., Rouabah, F., Mourad, A. I., Dadache, D., Magali, F., Houicha, H., Bencid, A.,* Citric acid treatment: A new approach to improving *Ampelodesma mauritanica* fibers-poly-lactic acid composites, Ind. Crop. Prod. **223** (2025) 120143.
doi: https://doi.org/10.1016/j.indcrop.2024.120143
47. *Ben Salem, D., Yahiaoui, K., Bernardo, M., Gatic, J. M., Ouakouak, A., Touahra, F., Eltaweil, A. S., Tran, H. N.,* Insights into cadmium adsorption characteristics and mechanisms by new granular alginate hydrogels reinforced with biochar: Important role of cation exchange, J. Environ. Manage. **383** (2025) 125407.
doi: https://doi.org/10.1016/j.jenvman.2025.125407
48. *Wong, S., Abd Ghafar, N., Ngadi, N., Razmi, F. A., Inuwa, I. M., Mat, R., Amin, N. S.,* Effective removal of anionic textile dyes using adsorbent synthesized from coffee waste, Sci. Rep. **10** (2020) 2928.
doi: https://doi.org/10.1038/s41598-020-60021-6
49. *Deivanayagam, P., Bhoopathy, R. P., Thanikarasan, S.,* Synthesis, characterization, antimicrobial, analgesic, and CNS studies of Schiff base Cu(II) complex derived from 4-choro-o-phenylene Diamine, Int. J. Adv. Chem. **2** (2014) 166.
doi: https://doi.org/10.14419/ijac.v2i2.3338
50. *Thommes, M., Kaneko, K., Neimark, A. V., Olivier, J. P., Rodriguez-Reinoso, F., Rouquerol, J., Sing, K. S. W.,* Physisorption of gases, with special reference to the evaluation of surface area and pore size distribution (IUPAC Technical Report), Pure Appl. Chem. **87** (2015) 1051.
doi: https://doi.org/10.1515/pac-2014-1117
51. *Sing, K. S. W.,* Reporting physisorption data for gas/solid systems with special reference to the determination of surface area and porosity, Pure Appl. Chem. **54** (1982) 2201.
doi: https://doi.org/10.1351/pac198254112201
52. *Touati, Z., de Hoyos-Martinez, P. L., Belhaneche-Bensemra, N., Charrier- El Bouhtoury, F.,* Influence of different diss fiber treatments over the properties of polypropylene/recycled and regenerated low-density polyethylene based biocomposites, J. Environ. Polym. Degrad. **29** (2021) 1.
doi: https://doi.org/10.1007/s10924-020-01877-7
53. *Khalfaoui, A., Benalia, A., Selama, Z., Hammoud, A., Derbal, K., Panico, A., Pizzi, A.,* Removal of Chromium(VI) from water using orange peel as the biosorbent: Experimental, modeling, and kinetic studies on adsorption isotherms and chemical structure, Water. **16** (2024) 742.
doi: https://doi.org/10.3390/w16050742
54. *Wang, Y., Eljamal, R., Nomura, T., Minami, E., Kawamoto, H.,* Thermal reactivities of hemicellulose and cellulose and demineralization effects on their reactivities in cell walls of various softwood and hardwood species, J. Wood Sci. **71** (2025) 39.
doi: https://doi.org/10.1186/s10086-025-02216-x
55. *Dixon, R. A., Barros, J.,* Lignin biosynthesis: Old roads revisited and new roads explored, Open Biol. **9** (2019) 190215.
doi: https://doi.org/10.1098/rsob.190215

56. *Akkari, I., Graba, Z., Pazos, M., Bezzi, N., Manseri, A., Derkaoui, K., Mehdi Kaci, M.,* NaOH-activated pomegranate peel hydrochar: Preparation, characterization and improved acebutolol adsorption, Water Air Soil Pollut. **234** (2023) 705.
doi: https://doi.org/10.1007/s11270-023-06723-9
57. *Wang, S., Luo, C., Tan, F., Cheng, W., Ma, Q., Wu, D., Li, P., Zhang, F., Ma, J.,* degradation of congo red by UV photolysis of nitrate: Kinetics and degradation mechanism, Sep. Purif. Technol. **262** (2021) 118276.
doi: https://doi.org/10.1016/j.seppur.2020.118276
58. *Chan, K. T., Ong, S. T., Ha, S. T.,* Adsorptive removal of Congo red dye from its aqueous solutions by tetraethylenepentamine modified peanut husk composite beads, Desalination Water Treat. **317** (2024) 100060.
doi: https://doi.org/10.1016/j.dwt.2024.100060
59. *Sanjabi, S., Salehiirad, A.,* $MgAl_2O_4$/$CoFe_2O_4$/Zeolite A magnetic ceramic nanocomposite for efficacious elimination of Methylene blue from aqueous solutions: Composition influence, Res. Chem. Intermed. **51** (2025) 4907.
doi: https://doi.org/10.1007/s11164-025-05679-1
60. *Semwal, N., Mahar, D., Chatti, M., Dandapat, A., Arya, M. C.,* Adsorptive removal of Congo Red dye from aqueous solution by Ag-Cu-CeO_2 nanocomposites: Adsorption kinetics, isotherms, and thermodynamics, Heliyon. **9** (2023) e22027.
doi: https://doi.org/10.1016/j.heliyon.2023.e22027
61. *Rangabhashiyam, S., Anu, N., Giri Nandagopal, M. S., Selvaraju, N.,* Relevance of isotherm in biosorption of pollutants by agricultural byproducts, J. Environ. Chem. Eng. **2** (2014) 398.
doi: https://doi.org/10.1016/j.jece.2014.01.014
62. *Debnath, S., Maity, A., Pillay, K.,* Impact of process parameters on removal of Congo Red by graphene oxide from aqueous solution, J. Environ. Chem. Eng. **2** (2014) 260.
doi: https://doi.org/10.1016/j.jece.2013.12.018
63. *Edet, U. A., Ifelebuegu, A. O.,* Kinetics, isotherms, and thermodynamic modeling of the adsorption of Phosphates from model wastewater using recycled brick waste, Proc. **8** (2020) 665.
doi: https://doi.org/10.3390/pr8060665
64. *Hatta, N. S. M., Hussin, F., Gew, L. T., Aroua, M. K.,* Isotherms, thermodynamics and regeneration studies of CO_2 adsorption on activated carbon impregnated with waste-sourced natural amino acids, Greenhouse Gases: Sci. Technol. **15** (2025) 472.
doi: https://doi.org/10.1002/ghg.2354
65. *Nguyen, C., Do, D. D.,* The Dubidin-Radushkevich equation and the underlying microscopic adsorption description, Carbon. **39** (2001) 1327.
66. *Zakhar, R., Derco, J., Čacho, F., Čižmárová, O.,* Adsorptive removal of pentavalent arsenic from aqueous solutions by granular ferric oxide, Chem. Biochem. Eng. Q. **36** (2022) 117.
doi: https://doi.org/10.15255/CABEQ.2021.2018
67. *Patl, P., Jeppu, G., Vallabha, M. S., Girish, C. R.,* Enhanced adsorption of phenolic compounds using biomass-derived high surface area activated carbon: Isotherms, kinetics, and thermodynamics, Environ. Sci. & Pollut. Res. **31** (2024) 67442.
doi: https://doi.org/10.1007/s11356-024-32971-1
68. *Chakraborty, P., Show, S., Banerjee, S., Halder, G.,* Mechanistic insight into sorptive elimination of ibuprofen employing bi-directional activated biochar from sugarcane bagasse: Performance evaluation and cost estimation, J. Environ. Chem. Eng. **6** (2018) 5287.
doi: https://doi.org/10.1016/j.jece.2018.08.017
69. *El-Nemr, M. A., Aigbe, U. O., Ukhurebor, K. E., Obodo, K., Awe, A. A., Hassaan, M. A., Ragab, S., El Nemr, A.,* Modelling of a new form of nitrogen-doped activated carbon for the adsorption of various dyes and hexavalent chromium ions, Sci. Rep. **15** (2025) 3896.
doi: https://doi.org/10.1038/s41598-025-87398-6
70. *Steinbrecher, T., Albert, J., Kaltschmitt, M.,* The nature of lignin and implications for its technical use as a source for biogenic aromatics- A review, Sustain. Chem. **6** (2025) 38.
doi: https://doi.org/10.3390/suschem6040038
71. *Wanyonyi, W. C., Onyari, J. M., Shiundu, P. M.,* Adsorption of Congo red from aqueous solutions using roots of *Eichhornia crassipes:* Kinetics and equilibrium studies, Energy Procedia. **50** (2014) 862.
doi: https://doi.org/10.1016/j.egypro.2014.06.105
72. *Ige, A. O., Ogunsile, B. O., Ore, O. T., Olawade, D. B.,* Adsorption of Congo Red from aqueous solution using rice husk, calcined kaolin clay, and microwaved rice husk clay hybrid, Discov. Chem. **1** (2024) 9.
doi: https://doi.org/10.1007/s44371-024-00010-0
73. *Harjal, M., Buema, G., Bucur, D.,* Recent advances in removal of Congo Red dye by adsorption using an industrial waste, Sci. Rep. **12** (2022) 6087.
doi: https://doi.org/10.1038/s41598-022-10093-3
74. *Tang, S. H., Zaini, M. A. A.,* Congo red removal by HNO_3-modified resorcinol formaldehyde carbon gels, Chem. Eng. Trans. **56** (2017) 835.
doi: https://doi.org/10.3303/CET1756140
75. *Hamd, A., Salah, D., Alyafei, H. F., Soliman, N. K., El-Reedy, A. A. M., Elzanaty, A. M., Al-Saeedi, S. I., Al-Ghamdi, A., Shaban, M., El-Sayed, R., Ahmed, S. A.,* NaOH-activated natural gluconite for low cost adsorption of Congo Red, Water. **15** (2023) 3753.
doi: https://doi.org/10.3390/w15213753
76. *Gkika, D. A., Liakos, E. V., Vordos, N., Kontogoulidou, C., Magafas, L., Bikiaris, D. N., Bandekas, D. V., Mitropoulos, A. C., Kyzas, G. Z.,* Cost estimation of polymeric adsorbents, Polym. **11** (2019) 925.
doi: https://doi.org/10.3390/polym11050925
77. *Esmati, F., Holliday, M. C., Zein, S. H., Jabbar, K. J., Tan, S. H., Putranto, A.,* Enhancing hexavalent chromium removal from textile effluent with low-cost adsorbent: Simulation and a techno-economic study, Int. J. Environ. Sci. Technol. **22** (2025) 6345.
doi: https://doi.org/10.1007/s13762-024-05958-1
78. *Mihret, T., Gabbiye, N., Tegegne, B., Tibebe, D., Alemu, A.,* Removal of reactive red 45 dye from aqueous solution using activated carbon developed from *Catha edulis* stem as a potential biosorbent, Sci. Rep. **15** (2025) 28195.
doi: https://doi.org/10.1038/s41598-025-09956-2
79. *Sahu, N., Nayak, A. K., Verma, L., Bhan, C., Singh, J., Chaudhary, P., Yadav, B. C.,* Adsorption of As(III) and As(V) from aqueous solution by magnetic biosorbents derived from chemical carbonization of pea Peel waste biomass: Isotherm, kinetic, thermodynamic, and breakthrough curve modeling studies. J. Environ. Manage. **312** (2022) 114948.
doi: https://doi.org/10.1016/j.jenvman.2022.114948
80. *Alalm, M. G., Nasr, M.,* Artificial intelligence, regression model, and cost estimation for removal of chlorothalonil pesticide by activated carbon prepared from casuarina charcoal, Sustain. Environ. Res. **28** (2018) 101.
doi: https://doi.org/10.1016/j.serj.2018.01.003
81. *Fouad, M., El-Fakharany, E. M., Mossad, M., Samy, M., Alalm, M. G.,* Persulphate activation by ferrous sulphate for tertiary treatment of real domestic wastewater to meet the standards of irrigating food crops, J. Water Proc. Eng. **75** (2025) 107961.
doi: https://doi.org/10.1016/j.jwpe.2025.107961